A primal role for balance in the development of coordinated locomotion

David E. Ehrlich and David Schoppik

Departments of Otolaryngology, Neuroscience & Physiology, and the Neuroscience Institute, New York University School of Medicine, New York, NY 10016

Mature locomotion requires that animal nervous systems coordinate distinct groups of muscles. The pressures that guide the development of coordination are not well understood. We studied vertical locomotion in developing zebrafish to understand how and why coordination might emerge. We found that zebrafish used their pectoral fins and bodies synergistically to climb. As they developed, zebrafish came to coordinate their fins and bodies to climb with increasing postural stability. Fin-body synergies were absent in mutants without vestibular sensation, linking balance and coordination. Similarly, synergies were systematically altered following cerebellar lesions, identifying a neural substrate regulating fin-body coordination. Computational modeling illustrated how coordinated climbing could improve balance as zebrafish mature. Together these findings link the sense of balance to the maturation of coordinated locomotion. As they develop, zebrafish improve postural stability by optimizing fin-body coordination. We therefore propose that the need to balance drives the development of coordinated locomotion.

Introduction

To locomote, the nervous system coordinates multiple effectors, such as the trunk and limbs or fins, that collectively generate propulsive forces and maintain body posture. For example, humans walk by using the legs to move the body forward, swinging the arms to reduce angular momentum, and using axial musculature to support the trunk [1]. As animals mature they change the way they coordinate these effectors, a process driven both by experience and by changing motor goals [2–4]. However, which sensations and goals guide the development of coordination is poorly understood. During development, both physical body shape and neural coordination change simultaneously [5]. Understanding the constraints that guide neural control of coordination therefore requires a model in which the maturation of locomotion can be dissociated from changes in physical form [6].

Development of coordination is simplified under water, where individual effectors function dissociably [7, 8]. Whereas forces generated while walking ultimately act through the feet, fish bodies and fins serve as independent control surfaces that need not be used in concert. For example, fish can climb in the water column using pectoral fins or body/caudal fin undulation, meaning a given climb can be executed with varying mechanics [9–11]. These mechanics can be defined with respect to common mechanics of flight (Figure 1A). Bodies that move in the direction they point – like a rocket – must direct thrust upwards by pitching upwards in order to climb [12]. Similarly, fish pitch upwards to direct thrust from the body/caudal fin, particularly fish with dorsoventrally symmetric bodies that generate minimal lift [13, 14]. In contrast, bodies that generate lift – like a helicopter with its rotor – can remain horizontal while climbing. Fishes can produce lift using their pectoral fins (see technical note in Methods) [9].

How fish coordinate their bodies and fins has direct consequences for balance. When a fish generates lift with its pectoral fins, it moves upwards relative to its body posture, creating an attack angle (Figure 1A). Division of labor among the body and fins therefore defines how far posture must deviate from horizontal in order to climb. Given that many fish actively balance near horizontal, even during the first days of swimming [15, 16], fin use may be preferable. Pectoral fin and body movements occur synchronously in larvae [17], but the fins appear dispensable for routine swimming in the roll and yaw axes at this stage [18]. We hypothesized that fish regulate fin-body coordination in the pitch (nose-up/nose-down) axis as they develop, learning to increasingly utilize their fins to better maintain balance as they climb.

To examine how and why fish regulate fin-body coordination across development, we studied larval zebrafish (*Danio rerio*) as they spontaneously climbed in the water column. We compared groups of siblings, or clutches, throughout the larval stage (3-30 days post-fertilization, dpf) [19]. Larvae locomote in discrete bouts approximately once per second, simplifying kinematic analysis [16, 20]. We found that larvae climbed with steeper trajectories than would be predicted from posture alone – evidence they were actively generating lift. After fin amputation, larvae no longer generated lift. We found that larvae at all ages exhibited synergy between fin-driven lift and body rotations, strong evidence for active coordination. Consistently, we found that fin-body coordination was abolished in vestibular mutants with an impaired sense of balance [21] and perturbed by cerebellar lesions. Developing larvae regulated fin-body coordination to rely increasingly on their fins during climbs. Consequentially, older larvae were observed to climb with balanced postures closer to horizontal. To understand why larvae at different ages coordinated their fins and bodies in different ways, we built a model to explore trade-offs between balance and effort, defined with respect to the underlying commands to control the fins and body [22, 23]. Simulations showed that more mature coordination, dominated

by pectoral fins, improved balance but cost greater effort. We conclude that developing zebrafish come to optimize fin-body coordination to stabilize posture while climbing. We therefore propose that a drive to balance guides the development of coordinated locomotion.

Results

Larvae use pectoral fins to balance while climbing

First we examined climbing kinematics late in the larval stage, from 2912 bouts captured from 45 larvae across 6 clutches at 3 weeks post-fertilization (wpf). Larvae tended to pitch upwards in order to swim upwards, yielding a positive correlation of trajectory and pitch-axis posture that reflected thrust-based climbing (Figure 1B; Spearman's $\varrho = 0.81$). In addition, larvae often swam with positive attack angles (defined here as the difference between trajectory and posture) that reflect the production of lift. They exhibited positive attack angles preferentially when climbing, in 92.5% of bouts with upwards trajectories (1866/2016). By comparison, larvae exhibited positive attack angles in only 13.8% of bouts when diving (124/896). Larvae therefore climb by pitching upwards and generating lift.

We hypothesized that larvae generated lift using their pectoral fins, because they tend to abduct the fins while swimming [24, 25] and did so when propelling upwards (Supplemental Movies 1 & 2). When we amputated the pectoral fins and recorded 1,890 bouts, we found that positive attack angles were largely abolished (Figure 1B). Control larvae exhibited attack angles of 15.6° on average, compared to -8.0° for finless siblings (Figure 1C; n=6 groups of 6-8 finless larvae, pairwise t-test: $t_5 = 4.55, p = 0.0061$). A finless larva simply propelled in the direction it pointed, exhibiting a trajectory that closely approximated its posture, albeit with a minor downward bias. Accordingly, finless larvae never made the near vertical climbs of control siblings (Figure 1B). Small negative attack angles exhibited by finless larvae are consistent with a slight negative buoyancy [26] and an observed tendency to sink between propulsive bouts (Supplemental Figure S1; Supplemental Movie 1). We conclude larvae at 3 wpf used their pectoral fins to generate lift.

Importantly, larvae effected thrust- and lift-based climbing independently. Pectoral fin amputation did not influence body rotations in the pitch axis (Figure 1B, Supplemental Figure S2) or swimming more generally (Supplemental Figure S3; consistent with [17]). Specifically, amputation had no significant effect on bout maximum speed (paired t-test, p>0.05, t_{10}=-1.14), displacement (t_{10}=-1.66), rate (t_{10}=0.23), or absolute pitch-axis rotation (t_{10}=1.25). We conclude that larvae do not require their pectoral fins to pitch upwards and climb, presumably instead rotating using the body and caudal fin [14, 27].

We hypothesized that larval pectoral fins are well suited for generating lift without torque because they attach near the body center of mass [28]. Pectoral fins would therefore act over a small moment arm to generate torques in the pitch axis, making those torques small. We measured the rostrocaudal positions of pectoral fin attachment from 15 larvae and compared those to morphometrically estimated positions of the center of mass [16]. Indeed, the pectoral fins attached consistently near the center of mass, on average 0.056±0.007 body lengths rostrally (Supplemental Figure S4). The position of the pectoral fins in larval zebrafish may therefore facilitate dissociation of lift- and thrust-based climbing, enabling larvae to specifically use pectoral fins to produce lift without causing pitch-axis body rotation.

Following pectoral fin amputation, larvae compensated for loss of lift by controlling their posture. Larvae rotated farther from horizontal in order to climb. In order to produce climbs steeper than 20°, finless larvae pitched significantly farther upwards than control siblings; they adopted postures of 23.5° compared to 16.5° (Figures 1D, 1E; pairwise t-test, $t_5 = 5.02, p = 0.0040$). Consistently, finless larvae were unable to produce steep climbs at horizontal postures, unlike control siblings. We conclude that use of the pectoral fins for climbing facilitates balance, enabling larvae to maintain postures near horizontal.

Larvae coordinate fins and bodies to climb

Larvae could facilitate climbing by combining independent lift- and thrust-based mechanisms (Figure 2A). Pairing fin-mediated lift with upwards posture changes would yield synergistic climbing effects. Conversely, lift from fins would interfere with diving produced by downwards posture changes. If larvae concertedly use both their fins and bodies to climb and dive, we would expect attack angles and postural control to be correlated.

To understand how developing larvae coordinated their fins and bodies, we examined concurrent control of these effectors during bouts. We measured swimming at 1, 2, and 3 wpf across 4 clutches (3552, 2326, and 693 bouts, respectively). Additionally, we examined their newly-swimming siblings at 4 days post-fertilization and found that fin use was indistinguishable from that at 1 wpf (4004 bouts, Supplemental Table 1).

First, we assessed how larvae used their bodies to direct thrust. Because larvae actively control their posture during swim bouts, we reasoned that they may acutely change posture in pitch to direct thrust up or down [16, 29]. To assess whether larvae changed posture before generating thrust, we compared the timing of angular and linear accelerations during spontaneous swim bouts. We found that larvae at all ages produced large, pitch-axis angular acceleration preceding and during thrust generation, when they accelerated forwards (Figure 2B). Angular acceleration lasted approximately 100 msec and peaked 62.5 msec before larvae ceased generating thrust

and began linear deceleration. We defined the steering-related posture change of a bout from 25 to 75 msec before linear deceleration, and observed that all larvae exhibited comparable posture changes (Supplemental Table 1; Two-way ANOVA, main effect of age: $F_{2,6} = 2.21, p = 0.19$; main effect of clutch: $F_{3,6} = 1.89, p = 0.23$).

Larvae used their fins and bodies synergistically, particularly during steep climbs. Larvae at all ages exhibited positively correlated attack angles and posture changes (Figure 2C), with Spearman's correlation coefficients of 0.27±0.08 at 1 wpf (mean±S.D. across clutches), 0.38±0.13 at 2 wpf, and 0.37±0.14 at 3 wpf (Supplemental Table 1). In particular, larvae paired large, upwards posture changes (>5°) with positive attack angles; of 210 bouts with such posture changes across all ages, 193 (92%) had positive attack angles (binomial test: p=1.5E-21, given 63.4% of all bouts had positive attack angles).

To confirm that young larvae also generated positive attack angles with pectoral fins, we examined the effects of fin amputation at 1 wpf. Large attack angles (greater than 15°) were rare but observable in control larvae at 1 wpf (3.8%, 81/2652 bouts). In contrast, large attack angles were nearly abolished in siblings following pectoral fin amputation (0.6%, 16/2630 bouts; n=6 groups of 7-8 finless larvae, pairwise t-test: $t_5 = 4.40, p = 0.0070$). We conclude larvae at all ages coordinated their fins and bodies in order to climb.

Developing larvae regulate fin-body coordination

At all ages larvae paired positive posture changes with positive attack angles, but younger larvae paired a given posture change with smaller attack angles (Figure 2C). As a first pass, we quantified the ratio of attack angles to posture changes during shallow climbs (with posture changes from 0° to 3°) using a robust slope estimate; with age, the ratio of attack angles to posture changes nearly tripled, from 0.71:1 at 1 wpf to 1.61:1 at 2 wpf and 2.00:1 at 3 wpf. We conclude that older larvae produced small climbs with greater contribution from the pectoral fins.

Conversely, larvae at all ages made the steepest climbs similarly, reflecting comparable physical capabilities. Larvae at all ages paired the largest posture changes (5°-10°) with comparable attack angles (10°-20°, on average). Attack angles reached an asymptote as a function of posture change (Figure 2C), which we interpret as a physical constraint on attack angle; after maximizing attack angle, larvae could only climb more steeply by rotating farther upwards.

Given that larvae at all ages swam at comparable speeds (Supplemental Table 1, Two-way ANOVA with main effects of age and clutch, $F_{2,6} = 0.94, p = 0.44$), we conclude that the pectoral fins produce consistent maximal acceleration in the dorsal direction throughout the larval stage. Consistently, pectoral fins maintained similar proportional lengths to the body at 1 wpf (0.098±0.010 body lengths), 2 wpf (0.110±0.008), and 3 wpf (0.114±0.008, n=15; Supplemental Figure S4, Supplemental Table 1; One-way ANOVA, $F_{2,42} = 13.19, p = 3.60E-5$). These data suggest that developing larvae do not become physically more capable of climbing with the fins.

Instead, developing larvae changed how they distributed labor among the body and fins. Older larvae used the largest attack angles to climb on a greater proportion of bouts than younger larvae. Larvae at 3 wpf paired 2-3° posture changes with large 15.2° attack angles; although larvae at 1 and 2 wpf were capable of generating large attack angles, they paired 2-3° posture changes with attack angles of 5.8° and 8.8°, respectively. Furthermore, older larvae exhibited near-maximal fin use (>10° attack angle) on a far greater proportion of bouts (5.4% at 1 wpf, 19.9% at 2 wpf, and 38.7% at 3 wpf). Accordingly, larvae exhibited gradually increasing attack angles with age (Figure 2C, *marginals*; main effect of age by Two-way ANOVA, $F_{2,6} = 9.46, p = 0.014$), with significantly smaller angles at 1 wpf (1.02°) than 3 wpf (8.11°, p=0.004; Tukey's posthoc test). Together, these data suggest changes to fin-body coordination, rather than physical ability, account for the nearly 8-fold increase in attack angles from 1 to 3 wpf.

To model how attack angle varied as a function of posture change, we fit data with sigmoids (Figure 2C). We used logistic functions comprising 4 parameters: one to capture sigmoid amplitude, another for sigmoid steepness, and two for location (see Methods). Three parameters (for sigmoid amplitude and location) did not significantly differ across ages, further support for the hypothesis that fin capacity is constrained across early development (Supplemental Table 1). In contrast, the dimensionless steepness parameter significantly varied with age.

Sigmoid steepness captured fin-body coordination throughout development, reflecting increasing engagement of the fins during climbs. We found that sigmoid maximal slope increased more than four-fold with age (from 2.9 at 1 wpf to 7.0 at 2 wpf and 12.0 at 3 wpf) after fixing the remaining 3 parameters at their means across ages (Figure 2D). We conclude that larvae at all ages were capable of the same range of attack angles, but older larvae paired large attack angles with smaller posture changes.

Sigmoid slope was sufficient to describe variations in climbing behavior across clutches of fish. We measured sigmoid slope for individual clutches at each age, combining data over two successive recording days for good sigmoid fits (Supplemental Figure S5). Sigmoid slope exhibited a significant positive correlation with mean attack angle (Figure 2E, Pearson's r=0.94, p=5.6E-6) but not mean trajectory (r=0.29, p=0.28) or the frequency of steep climbs (r=0.40, p=0.13). Furthermore, sigmoid slope reflected clutch differences in development of fin use; only clutches with increased sigmoid slope from 2 to 3 wpf displayed increased attack angle (Figure 2E). These data suggest larvae swam with more lift while making the same climbs simply by biasing the composition of fin-body

coordination towards the fins.

Sigmoid slope was also correlated with a drive to maintain the preferred horizontal posture, suggesting larvae bias towards fin use to better balance. Slope exhibited a significant negative correlation with absolute deviation from horizontal (Figure 2F, r=-0.74, p=6.3E-3). During climbs steeper than 20°, larvae at 1 wpf adopted postures pitched significantly more upwards (28.0°; Two-way ANOVA, main effect of age: $F_{2,6} = 25.29, p = 0.0012$) than larvae at 2 wpf (19.7°; Tukey's test, $p = 0.0040$) or 3 wpf (17.7°; Tukey's test, $p = 0.0013$). Sigmoid slope also reflected clutch differences in development of balance; the lone clutch exhibiting a large decrease in sigmoid slope from 2 to 3 wpf (from 9.0 to 6.4) also exhibited worse balance, with larger deviation from horizontal at 3 wpf (11.0°) than at 2 wpf (8.6°; Figure 2F). Regardless of age, larvae that preferentially used their fins to climb remained nearer horizontal. We conclude that a single parameter captures variability of fin-body coordination across development and its consequences for balance.

Fin-body coordination requires vestibular sensation

To confirm that correlated fin and body actions arose due to coordination rather than biomechanics, we tested whether fin-body correlations were influenced by sensory perturbation. We examined swimming in larvae with genetic loss of function of utricular otoliths, sensors of head/body orientation relative to gravity [30]. Utricular otolith formation is delayed from 1 to 14 dpf by loss-of-function mutation of *otogelin* [21, 31] (Figure 3A). *otogelin* is expressed exclusively in cells in the otic capsule [32] where it is required for tethering of the otolith to the macula [33].

We found that correlated fin- and body-mediated climbing was abolished in *otog-/-* larvae. Mutants exhibited no correlation of attack angle and posture change across 3,656 bouts (Figure 3B; Spearman's $\varrho = 0.03, p = 0.051$; n=56 larvae from 5 clutches). In contrast, control siblings with functioning utricles exhibited a significant, positive correlation of attack angle and posture change across 4,767 bouts ($\varrho = 0.15, p = 2.01E-26$). The correlation between attack angle and posture change was significantly lower in *otog-/-* larvae than controls from the same clutch, assessed by pairwise t-test (t_4=4.01, p=0.016). Accordingly, maximal slope of the best-fit sigmoid to attack angle and posture change was significantly lower for mutants than controls and indistinguishable from zero (Figure 3C; with 95% CI: 0.07±0.09 vs. 1.11 ± 0.13). Furthermore, *otog-/-* larvae failed to pair large, upwards posture changes (> 5°) with positive attack angles; of 144 bouts with such posture changes, only 90 had positive attack angles (binomial test: p=0.215, given that 66.0% of bouts had positive attack angles). By comparison, control siblings exhibited positive attack angles on 112 of 141 bouts with large, upwards posture changes (binomial test: p=5.2E-8, given that 57.9% of bouts had positive attack angles). We conclude that correlated actions of the fins and body are generated by the nervous system using sensory information, and therefore constitute coordination.

As expected from the restricted pattern of gene expression, deficits in *otog-/-* larvae appeared to be specific to the sensory periphery. Mutants have no reported defects in the central nervous system [21] and appeared morphologically unaffected. We observed typical morphology of the body and pectoral fins (0.43±0.03 mm fin length vs. 0.42±0.04 mm for controls; n=15; $t_{28} = 0.80$, p=0.43; Supplemental Table 2). Consistently, distributions of attack angles were comparable for *otog-/-* larvae (1.6±5.2°) and siblings (1.1±6.6°; Figure 3B, *marginals*), suggesting they are capable of generating lift with the fins but fail to do so when climbing with the body. Validating direct comparison of climbing kinematics between mutants and control siblings, we found that *otog-/-* larvae made steep climbs (> 20°) as frequently as control siblings with utricles (35±13% vs. 23±9% for controls; pairwise t-test, $t_4 = 1.89$, $p = 0.13$) and could generally balance, orienting approximately horizontally on average in the light (8.35°). Gross swimming properties were also similar between *otog-/-* larvae and controls (Supplemental Table 3).

Like finless larvae, vestibular mutants that failed to coordinate their fins and bodies deviated farther from horizontal. Posture changes by *otog-/-* larvae were directed significantly more upwards than those by control siblings (Figure 3D; pairwise t-test, $t_4 = 3.13, p = 0.035$), which presumably compensates for less lift while climbing. Accordingly, *otog-/-* larvae exhibited significantly larger deviations from horizontal during climbs steeper than 20° (Figure 3E; 31.4±4.9° vs. 24.3±2.5° for controls; $t_4 = 3.02, p = 0.039$). We conclude that loss of fin-body coordination necessitates larger deviations from horizontal to climb.

The cerebellum facilitates fin-body coordination

The cerebellum is canonically involved in motor coordination and vestibular learning [34, 35] and cerebellar circuitry is largely conserved among vertebrates [36, 37]. We hypothesized that the zebrafish cerebellum facilitates fin-body coordination. To test this hypothesis we lesioned cerebellar Purkinje cells using the photosensitizer, KillerRed [38]. Purkinje cells are a necessary conduit for cerebellar information flow, providing sole innervation of cerebellar output neurons and themselves directly innervating the vestibular nuclei [37, 39]. We restricted KillerRed expression using the gal4:UAS system with a selective driver in Purkinje cells Tg(aldoca:GAL4FF) [40]. After light exposure, we measured swim bout kinematics (602 from 6 larvae) and compared them to bouts from unexposed KillerRed+ siblings (408 from 10 larvae). Swim kinematics were largely unaffected by Purkinje cell lesions (Supplemental Table 3) but postures tended nose-up (17.7±20.6° vs. 8.3±17.5° for controls).

Fin-body coordination was perturbed in larvae with Purkinje cell lesions. These larvae exhibited more positive attack angles than controls (Figure 4A; 3.83° vs. 0.82°; Kolmogorov-Smirnov test, p=1.6E-11), with comparable values to wild-type larvae a week older. Specifically, larvae with lesions exhibited positive attack angles during bouts with nose-down posture changes. Typically, larvae at all ages suppressed positive attack angles while rotating nose down. Given that positive attack angles reflect lift generation by the fins, and nose-down posture changes direct thrust downwards, such fin and body actions are conflicting.

To determine the probability that larvae performed conflicting fin-body actions, we identified bouts with nose down posture changes (<-1°) and measured the proportion with attack angles more positive than baseline (-1.59°, from wild-type fits at 1 wpf, Supplemental Table 1). Control larvae performed conflicting actions significantly less frequently than chance (Figure 4B; 0.429±0.071, with 95%CI), and larvae with lesions performed conflicting actions significantly more frequently than chance (0.642±0.121). Larvae with lesions were also significantly more likely to perform synergistic fin-body actions, pairing positive attack angles with nose-up posture changes (Figure 4C; 0.844±0.053 vs. 0.736±0.050 for controls).

Importantly, larvae with lesions exhibited more positive attack angles when making larger magnitude posture changes, be they nose-up or -down (Figure 4A). In order to quantify the relative magnitude of attack angles to both positive and negative posture changes, we modeled these data as the sum of two sigmoids, one of which was reflected about the vertical axis. Best-fit sigmoids captured the tendency to engage the fins during large positive and negative posture changes. For larvae with Purkinje cell lesions, the largest magnitude slope of the nose-down sigmoid significantly differed from 0 (Figure 4D; -4.09). Furthermore, that slope did not significantly differ in magnitude from the slope of the best-fit nose-up sigmoid (Figure 4E; 6.50). In contrast, the double sigmoid was overparameterized for fitting control data, and the maximal slope of the nose-down sigmoid did not differ from 0 (Figure 4D; -0.22; see Methods). Finally, the slope of the nose-up sigmoid was significantly larger for larvae with Purkinje cell lesions compared to controls (Figure 4E; 6.50 vs. 1.69). We conclude that the cerebellum actively suppresses fin-mediated lift generation during pitch-axis steering. Our data suggest a dual role for cerebellar regulation of fin-body coordination: to bias division of labor towards the body, and to prevent the production of conflicting fin-body actions.

A generative model of fin-body coordination

Why do developing larvae change how they divide labor between the fins and body? In other words, what cost function are larvae optimizing when they regulate fin-body coordination? To address this question, we built a simple computational model that allowed us to parameterize the division of labor between the fins and body (Figure 5A, details in Methods). In this control-theoretic model, a larva swam towards a target (up or down) by comparing the target's direction to the direction it would swim without steering (its current posture). From this difference the larva generated a steering command. The larva steered its swim bouts by using its fins to generate lift and its body to direct thrust.

Simulated larvae coordinated their fins and bodies by controlling both effectors with a mutual command. To vary the ratio of fin and body actions (attack angles and posture changes, respectively), the command was differentially scaled for the fins and body. Commands to the fins were weighted by a fin bias parameter ($0 \leq \alpha \leq 1$) and commands to the body by $(1-\alpha)$. Effector-specific commands were therefore positively correlated (when $\alpha \neq 0$ and $\alpha \neq 1$) in a ratio equal to $\alpha/(1-\alpha)$. Given this formulation, we could infer empirical fin biases ($\hat{\alpha}$) from the ratio of empirical attack angles and posture changes, given by sigmoid slope ($\hat{\alpha}$=slope/(1+slope); eq. 3). Empirical fin bias increased significantly with age (from 0.74 at 1 wpf to 0.92 at 3 wpf) like sigmoid slope, but ranged from 0 to 1 (Figure 5B; Supplemental Table 1).

Commands were transformed into kinematic variables according to physical transfer functions (Figure 5A) that increased approximately linearly near the origin, such that weak commands were faithfully transformed to movement; for large positive and negative commands, transfer functions reached asymptotes to model physical limitations. The asymptotes imposed empirically-derived constraints on the range of posture changes (-17.0 to +13.2°) and attack angles (-2.9 to +14.0°) of each bout. Additionally, Gaussian noise was added to swim trajectory to model errors in motor control and effects of external forces like convective water currents that move larvae (ε).

The model permitted simulation of larvae across development, because sigmoid slope (and therefore fin bias) captured developmental changes to swimming. We simulated larvae from each age group (100,000) identically, save for age-specific $\hat{\alpha}$, as they climbed in series of bouts until reaching targets positioned half the tank away (25 mm). We placed the targets in directions randomly drawn from observed climbing trajectories (see Methods). Simulated attack angles and posture changes were sigmoidally related, with steeper sigmoid slopes for older larvae (Figure 5C). Simply by varying fin bias, simulated larvae exhibited mean attack angles comparable to empirical values (Figure 5D). Simulated attack angles at age- and clutch-specific $\hat{\alpha}$ yielded close approximations of attack angle (R^2=0.79). A model with a single parameter that scales divergent commands can therefore produce fin-body coordination and mimic climbing behavior across development.

Increasing fin bias improves balance but costs effort *in silico*

Next we varied fin bias to assess direct consequences of fin-body coordination for balance and climbing efficacy. The model allowed us to simulate larvae that climbed solely by generating lift ($\alpha = 1$) or solely by changing their posture ($\alpha = 0$), the former yielding larvae that never deviated from horizontal (Figure 6A). As fin bias increased, larvae remained closer to horizontal while climbing. After 5 bouts towards the steepest drawn target (63°), larvae swimming without using their fins ($\alpha = 0$) deviated 52° from horizontal, larvae with small fin bias (like those at 1 wpf, $\hat{\alpha} = 0.74$) deviated 39°, and larvae with large fin bias (like those at 3 wpf, $\hat{\alpha} = 0.92$) deviated only 13°.

By parameterizing fin bias, we found that simulated deviations from horizontal were comparable to empirical values (Figure 6B). Larger fin biases were associated with smaller deviations from horizontal, reflecting better balance. Although the model was not explicitly fit to postural variables, simulated deviations from horizontal explained 48% of empirical variance for clutches and time-points across development (with fin biases spanning from 0.60 to 0.93). Additionally, at fin biases below 0.5, simulated deviations were consistent near 17°. *otog-/-* larvae exhibited very small fin bias ($\hat{\alpha} = 0.06$) and large deviations from horizontal similar to simulated values at low α (19.1°). We conclude that simulations accurately captured the consequences of fin bias for balance, with greater fin bias allowing larvae to remain nearer horizontal.

To quantify how fin bias affected swimming efficacy when climbing to targets, we measured effort. Because the specific form an effort term should take is unknown, we defined effort as the sum of squared motor commands for steering, after [22, 41]. There, the definition of effort was chosen to ensure a quadratic increase with the control signal. Increasing fin bias had opposite consequences for swimming effort, as larger fin biases made climbing more effortful. Larvae climbed farther at low fin biases, benefiting from the cumulative effects of posture change (Figure 5A). Simulated larvae at 1 wpf gained two-thirds more elevation (4.25 mm) than larvae at 3 wpf (2.55 mm) and nearly three times as much as larvae swimming solely with the fins ($\alpha = 1$, 1.54 mm).

Effort increased monotonically with fin bias (Figure 6C). Steering solely with the fins ($\alpha = 1$) required 32 times more effort, on average, than steering solely by rotating the body ($\alpha = 0$). By evaluating simulated effort at empirical fin biases, we estimated that older larvae swam with greater effort; efforts at empirical fin biases (relative to effort at $\alpha = 1$) corresponded to 3.6%, 5.5%, and 7.9% at 1, 2, and 3 wpf, respectively (Figure 6C, triangles). Further, very small fin bias observed in *otog-/-* larvae approximately corresponded with the least effortful swimming (3.1% of effort at $\alpha = 1$). Results were qualitatively similar when computing effort as the sum of squared kinematic variables (posture change and attack angle), rather than commands (data not shown). We conclude that larvae achieve the least effortful climbing at low fin biases, and swim with increasing effort as they develop.

Given that balance and effort placed opposing demands on fin-body coordination, we composed cost functions from terms for both balance and effort (Figure 6D). Specifically, we tested whether combinations of balance and effort terms could prescribe specific fin biases for optimal swimming. Cost functions are inherently dimensionless, so we summed normalized curves for balance (deviation from horizontal as a function of α, Figure 6B) and effort (sum of square motor commands as a function of α, Figure 6C). To vary the relative importance of balance and effort terms, we weighted them by β (balance weight) and 1-β, respectively.

We parameterized β and found the optimal fin bias ($\alpha^*(\beta)$), the fin bias at which cost was minimized (Figure 6E). As β increased and cost functions grew more similar to deviation from horizontal, cost was minimized at larger fin biases. When $\beta = 0$ and the cost function was identical to effort, the optimal fin bias was that which minimized effort ($\alpha * (0) = 0.24$). Conversely, maximal fin bias was optimal for a range of cost functions that heavily weighted balance ($\beta > 0.72$).

At each age larvae appeared to swim optimally, given differential weights for balance and effort. Empirical fin biases minimized distinct cost functions composed from different balance weights (Figure 6E). From the cost functions that were minimized by empirical fin biases, we estimated the inferred balance weight ($\hat{\beta}$) at each age. Fin bias of larvae at 1 wpf minimized a cost function composed from a very low inferred balance weight (Figure 6F) $\hat{\beta} = 0.12$). Inferred balance increased by 2 wpf and significantly by 3 wpf, to 0.18 and 0.32, respectively. By providing a framework to contextualize our observations, the model offers a way to understand the trade-offs facing developing larvae. We conclude that larvae regulate fin-body coordination to optimize balance and effort, and that development of fin-body coordination can be explained by an increase in the importance of balance relative to effort.

Discussion

Here we used a new model to study coordinated movements and discovered a fundamental role for balance in the development of locomotion. First, we demonstrated that to climb, zebrafish larvae used upward-orienting body rotations and lift-producing pectoral fin actions. Larvae actively coordinated two independent effectors, the trunk and the pectoral fins, to locomote upward. As they developed, larvae came to match larger fin actions with smaller body rotations. The increasing reliance on fin-mediated climbing facilitated postural stability. Gravity-blind larvae did not coordinate the trunk and fins de-

spite performing similar body and fin actions, linking sensed posture to coordination. Cerebellar lesions produced systematic changes to fin and body coordination, revealing a neural substrate for regulation of fin-body coordination. Increasingly stable posture came at a cost as animals developed: the effort necessary to climb using fins. A generative model of locomotor development allowed us to explore the trade-offs between effort and balance. These simulations quantified the increasing importance of balance as fish grow. Taken together, our data show how the drive to balance comes to shape the development of coordinated locomotion.

Previous work using larval zebrafish examined pectoral fin kinematics during yaw and roll turns [17, 18]. Few differences were observed in yaw and roll between wild-type fish and mutants lacking pectoral fins. Instead, observed pectoral fin movements *between* bouts led the authors to propose the intriguing hypothesis that pectoral fin movements played a role in respiration. Complementarily, we find that larvae use their pectoral fins during climbing bouts to generate lift. Our data establish a novel locomotor function for pectoral fins in larval zebrafish, providing a more complete picture of their utility.

Climbing mechanics are well-established for adult fishes [9, 28, 42]. While we define a role for the pectoral fins in larval zebrafish climbing, the relevant kinematics remain unknown. Our work establishes several important constraints on the maturation of pectoral fin function. First, fin loss had no apparent impact on the ability of larvae to rotate their bodies in the pitch axis. Consistently, we observed that pectoral fins were located rostrocaudally near the estimated body center of mass, yielding a small moment arm in the pitch axis [28]. Second, across development, larvae exhibited similar maximal attack angles, suggesting that, as would thrust [43], lift forces scaled with body mass as larvae developed. Comparable function of the pectoral fins with age may reflect their musculoskeletal simplicity in larvae [18, 44]. In contrast to larvae, mature fish use their pectoral fins both to steer and as proprioceptors [45, 46]. Future work relating pectoral fin kinematics to vertical wake structure in developing zebrafish stands to illuminate how morphological maturation permits increasingly sophisticated movements across development.

We found that larval zebrafish coordinated their pectoral fins and bodies, controlling them independently but using them synergistically to facilitate climbing. Importantly, larvae missing their utricular otoliths, i.e. gravity-blind mutants [21], did not coordinate fin and body actions despite performing each typically. Two important conclusions follow from the mutant experiments. First, coordination of fin and body movements reflects patterned control, distinct from movements that are correlated simply due to biomechanics [47]. Second, though gravity-blind mutants could swim with a normal dorsal-up orientation in the light, utricular information is necessary for proper coordinated climbing. In mutant fish, posture changes and attack angles were normal, but unrelated. Synergistic fin and body movements therefore reflect a neural transformation of vestibular information into coordinated commands for climbing.

Our discovery that loss of the utricular otoliths abolishes fin and body synergy reveals a vestibular origin for the signals guiding coordinated climbing. On land, animals can infer their orientation relative to gravity from sensed pressure and muscle tension, allowing touch and proprioception to guide posture and locomotion [48, 49]. In zebrafish, recent work has identified a class of spinal proprioceptors that provide feedback during axial locomotion [50], and ascending feedback from the spinal cord in swimming tadpoles can drive compensatory ocular reflexes [51]. However, under water, the homogeneous physical environment necessitates vestibular strategies to guide coordinated locomotion with respect to gravity – such as the climbs we have studied here. Links between the vestibular system and postural orientation in the pitch axis are present in evolutionarily ancient vertebrates such as lamprey [52]. Vestibular information can drive pectoral fin movements in chondrichthyes [53], one of the earliest classes in which pectoral fins appear [54]. Considerable morphological [55] and molecular [56] work underscores the importance of the pectoral fins in the evolution of terrestrial appendages and gaits necessary for locomotion. Our findings extend this work by linking sensed gravity to the underwater climbing behaviors these ancient appendages serve.

Existing literature suggests a neural substrate for the vestibular signals that promote coordination. The utricles transduce body orientation and self-motion but are insensitive to vertical forces orthogonal to the utricular macula [57, 58], and should therefore be irrelevant for execution or perception of lift forces directly. A central origin for the signals that guide coordination is therefore more plausible, specifically in the utricle-recipient hindbrain vestibular nuclei [27, 59]. One of these, the tangential nucleus, contains "Ascending-Descending" neurons [60]. These neurons are distinguished by bifurcating axons that project rostrally, ascending to a midbrain nucleus, the nucleus of the medial longidutinal fasciculus, a region responsible for descending control of swim kinematics [61–63]. Ascending-Descending neurons are anatomically poised to also relay otolith-derived signals to the pectoral fins, as they make descending projections to th e locus of the pectoral fin motoneurons: the caudal hindbrain/rostral spinal cord [64]. Pectoral fin motoneurons have been studied in the context of axial swimming, and this work has established that rostral hindbrain-derived signals are important for proper pectoral fin control during fast swimming [25]. In order to convey feedback to pectoral motoneurons about pitch-axis postural changes, Ascending-Descending neurons would need to en-

code angular velocity, consistent with the transient responses to pitch-axis posture changes of neurons in the fish tangential nucleus [65] and with hindbrain vestibular responses more broadly [66]. Ascending-Descending neurons in the tangential vestibular nucleus are therefore a likely substrate by which utricular information comes to regulate fin-body coordination.

The cerebellum has long been recognized for its role both in enabling [67] and learning [68, 69] coordinated movements, though the computations responsible remain contentious [70]. We found that ablation of cerebellar Purkinje cells perturbed fin-body coordination, leading to the production of conflicting actions in which larvae generated fin-mediated lift while making nose-down rotations. Furthermore, ablation changed fin-body coordination during nose-up rotations, causing larvae to pair stronger fin actions with the same body rotation. We conclude that the cerebellum acts to suppress lift generation by the fins during body rotations, and thereby prevents the production of conflicting actions. Purkinje cells in the lateral cerebellum of zebrafish, labeled in the driver line used here [40], project to vestibular nuclei [71] and respond to rotational visual stimuli [72] and vestibular stimulation [73, 74]. Intriguingly, cerebellar lesions in the dogfish result in profound impairment of pectoral fin reflexes [75]. Combining quantitative measurements of locomotion and molecularly-targeted perturbations has begun to yield new insights into cerebellar function [76]. Similarly, climbing in zebrafish will likely prove to be a uniquely tractable entry point into the study of the cerebellum's role in the development of coordinated locomotion.

The development of fin-body coordination may specifically reflect changes to sensory perception / processing, as opposed to motor capacity. Support for this proposal comes from our observation that uncoordinated gravity-blind mutants can use their fins as well as their wild-type counterparts, suggesting a fully-capable motor system. Further, young larvae were physically capable of producing large attack angles with the fins synergistically rotating their bodies to climb. Finally, the range of body rotations larvae produced did not change across development. Therefore, development does not require unlocking or composing new actions, but instead involves selecting a particular combination of equally functional innate actions [2, 77]. As in other vertebrates [78], the capacity of the vestibular system to stabilize gaze [60] and posture [16] improves markedly with age. In mature animals, vestibular information is thought to be weighted by reliability for perceptual computations [79], consistent with learning rules [80] that may underlie locomotor development. We propose that fundamental limit on locomotor development reflect not motor capabilities, but peripheral or central limits to perceived posture.

We hypothesized that the development of coordination is an adaptive process driven by dynamic optimization rules [81]. To explore how larvae might implement these rules, we utilized simulations to quantify and compare the effects of coordination parameters on performance variables: not only accuracy, but also effort and balance [23, 82]. Because the fins and body were redundant, accuracy constraints did not prescribe a specific division of labor. Steering with the body had a distinct advantage: rotations reoriented the body towards the target, minimizing the need for subsequent steering. Further, the more a larva used its pectoral fins to climb, the more effort (defined as the sum of the square of the inferred motor commands) it expended to reach its target. However, steering with fins facilitated balance, because the fins enabled climbing without changing trunk posture. We conclude that body-dominated climbing of young larvae is optimized primarily for effort – or a variable that similarly scales with the sum of the control signals – while fin-body synergies of older larvae are optimized both for effort and balance. In this light, larvae at all ages may be considered equally skilled, with motor skill defined as the extent of optimization, and maturation considered a reflection of changing constraints on movement [83].

Considerable effort has gone into defining the fundamental principles by which coordination emerges during locomotor development [84, 85]. Maturation of coordination is thought to permit optimization of locomotion based on experience, and to facilitate adaptations to changing motor goals [2–4]. Further, mature patterns of locomotion may be generally disfavored until balance can be maintained [86–89]. However, the complexity of terrestrial biomechanics has made it difficult to understand why animals change the way they locomote, and how they accomplish these changes. We studied a simpler system – climbing underwater – to disentangle corporeal development from locomotor maturation. We discovered that the vestibular system shapes synergies between fin and body actions as larval fish learn to climb. Our work demonstrates the fundamental importance of balance for the development of coordinated locomotion.

Materials and Methods

Fish husbandry and lines

Procedures involving larval zebrafish (*Danio rerio*) were approved by the Institutional Animal Care and Use Committee of New York University. Fertilized eggs were collected from in-crosses of a breeding population of Schoppik lab wild-type zebrafish maintained at 28.5°C on a standard 14/10 hour light/dark cycle. Before 5 dpf, larvae were maintained at densities of 20-50 larvae per petri dish of 10 cm diameter, filled with 25-40 mL E3 with 0.5 ppm methylene blue. Subsequently, larvae were maintained on system water in 2 L tanks at densities of 6-10 per tank and fed twice daily. Larvae received powdered food (Otohime A, Reed Mariculture, Campbell, CA) until 13

dpf and brine shrimp thereafter. Larvae were checked visually for swim bladder inflation before all behavioral measurements.

Transgenic fish with loss-of-function mutation of the inner ear-restricted gene, *otogelin* (*otog-/-*), which exhibit delayed development of utricular otoliths (rock solo^{AN66} [90]. Homozygous offspring were visually identified by lack of utricular otoliths at 2 dpf, and confirmed to have typical posterior position and morphology of saccular otoliths. For behavioral comparison siblings with unaffected otoliths were used.

Transgenic fish expressing KillerRed in Purkinje cells were generated using the *aldoca:GAL4FF* line [40], by crossing to *UAS:KillerRed* [38].

Morphological measurement

Dorsal-perspective, bright-field photomicrographs of 15 wild-type larvae across three clutches were taken at each developmental time-point using an 8 megapixel iSight camera (Apple) through the ocular of a stereoscope (M80, Leica Microsystems). Larvae were immobilized dorsal up in 2% low-melting temperature agar (Thermo Fisher Scientific 16520). Body length and rostrocaudal position of the pectoral fin base were measured in Fiji [91] and compared to previously published estimates of center of mass (COM), estimated by modeling bodies as series of elliptic cylinders [16]. Additionally, body and pectoral fin lengths were measured from 15 *otog-/-* larvae and 15 phenotypic controls (*otog*+/- or *otog*+/+, differentiated by absence of utricles) at 1 wpf.

Surgery

Pectoral fins were amputated from wild-type larvae anesthetized in 0.02% ethyl-3-aminobenzoic acid ethyl ester (MESAB, Sigma-Aldrich E10521, St. Louis, MO). Pairs of anesthetized, length-matched siblings were immobilized dorsal-up in 2% low-melting temperature agar (Thermo Fisher Scientific 16520), and both pectoral fins of one larva were removed by pulling the base of the fin at the scapulocoracoid laterally with forceps. Then, both siblings were freed from the agar with a scalpel and allowed to recover in E3 for 4-5 hours prior to behavioral measurement.

Cerebellar lesion

Cerebellar Purkinje cells were lesioned at 6 dpf specifically using transgenic expression of the photosensitizer, KillerRed. Larvae were mounted dorsal-up in agarose and anesthetized in MESAB. Control, transgenic fish were anesthetized in MESAB in parallel. Illumination conditions on a widefield microscope (Axio Imager M1, Zeiss, Oberkochen, Germany) were set under blue light (480/30 excitation filter from filter set 19002, Chroma Technology, VT) to visualize but not activate KillerRed. Light was focused through a 40x, 0.75NA water immersion objective (Zeiss Achroplan), stopped down to fill a 0.3 mm diameter region, and focused on the Purkinje cell somata. Green light (540/25 excitation filter from filter set 19004, Chroma Technology, VT) was then applied for 15 min, quenching KillerRed fluorescence. The power at the sample plane, measured at 540nm with a 9.5mm aperture silicon photodiode (PM100D power meter, S130C sensor, Thorlabs, NJ) was 14mW. Fish were allowed to recover for 16-24 hours before behavioral measurements.

Behavior measurement

Experiments were performed on 4 clutches of 32 wild-type siblings, with 8 larvae per clutch recorded at 4 dpf and 1, 2, and 3 wpf as in a previous study [16]. Additionally, 12 clutches of 12-16 larvae each were divided evenly and compared with and without amputation of the pectoral fins, both at 1 and 3 wpf (6 clutches each). Five clutches of 16 siblings each, 8 lacking utricles (*otog-/-*) and 8 phenotypic controls (*otog*+/- or *otog*+/+), were measured at 1 wpf before homozygous mutants develop utricles [27]. Finally, 16 *Tg(aldoca:GAL4FF;);Tg(UAS:KillerRed)* siblings, 10 lesioned and 6 controls, were measured at 1 wpf in constant darkness.

Larvae were filmed in groups of 4-8 siblings in a glass tank (93/G/10 55x55x10 mm, Starna Cells, Inc., Atascadero, CA, USA) filled with 24-26 mL E3 and recorded for 48 hours, with E3 refilled after 24 hours. The thin tank (10 mm) restricted swimming near the focal plane. Water temperature was maintained at 26°C in an enclosure with overhead LEDs on a 14/10 hour light/dark cycle. Video was captured using digital CMOS cameras (BFLY-PGE-23S6M, Point Grey Research, Richmond, BC, Canada) equipped with close-focusing, manual zoom lenses (18-108 mm Macro Zoom 7000 Lens, Navitar, Inc., Rochester, NY, USA) with f-stop set to 16 to maximize depth of focus. The field-of-view, approximately 2x2 cm, was aligned concentrically with the tank face. A 5W 940nm infrared LED backlight (eBay) was transmitted through an aspheric condenser lens with a diffuser (ACL5040-DG15-B, ThorLabs, NJ). An infrared filter (43-953, Edmund Optics, NJ) was placed in the light path before the imaging lens.

Video acquisition was performed as previously [16]. Digital video was recorded at 40 Hz with an exposure time of 1 ms. To extract kinematic data online using the NI-IMAQ vision acquisition environment of LabVIEW (National Instruments Corporation, Austin, TX, USA), background images were subtracted from live video, intensity thresholding and particle detection were applied, and age-specific exclusion criteria for particle maximum Feret diameter (the greatest distance between two parallel planes restricting the particle) were used to identify larvae in each image [16]. In each frame, the position of the visual center of mass and posture (body orientation in the pitch, or nose-up/down, axis) were collected. Posture was defined as the orientation, relative to horizontal, of the line passing through the visual centroid that minimizes the visual moment of inertia, such that a larva with posture zero has its longitudinal axis horizontal.

Supplemental videos at high spatial resolution were alternatively filmed in a thinner glass tank (96/G/5 24x5x5 mm, Starna Cells, Inc.) using a Sony IMX174 CMOS chip (ace acA1920-155um, Basler AG, Germany) equipped with a high-magnification fixed focus lens (Infinistix 0.5x, Infinity Optical Company, Boulder CO) and a high-pass infrared filter (Optcast 43948, Edmund Optics). Infrared illumination was provided by multiple high-power LEDs (5W 940nm center wavelength, eBay); one, mounted behind the tank, provided transmitted light, passed through an aspheric condenser lens with diffuser (ACL5040-DG15-B) and a piece of Cinegel #3026 Filter paper (Rosco USA, Stamford CT). Three additional infrared LEDs were mounted between the lens and the tank to provide reflected illumination: one coupled to a fiber optic ring light (Optcast 54176, Edmund Optics) mounted on the lens barrel, and two additional bare LEDs mounted on either side of the tank at 45°angles. Full-frame (1900x1200, 8-bit) video capture was triggered at 60 Hz with a 7ms exposure time.

Behavior analysis

Data analysis was performed using Matlab (MathWorks, Natick, MA, USA). Epochs of consecutively saved frames lasting at least 2.5 sec were incorporated in subsequent analyses if they contained only one larva. Data were analyzed from the light phase during the first 24 hours of measurement, but excluded a 2 hour period following transition from the dark phase to minimize influence of light onset.

Deviation from horizontal was computed as the mean of absolute value of all postures observed. Instantaneous differences of body particle centroid position across frames were used to calculate speed. As previously [16], bouts were defined as periods with speeds exceeding 5 mm·sec^{-1}, and consecutively detected bouts faster than $13\frac{1}{3}$ Hz were merged.

Numerous properties of swim bouts were measured or calculated. The maximum speed of a bout was determined from the largest displacement across two frames during the bout. The trajectory of a bout was defined as the direction of instantaneous movement across those two frames. Bouts with backwards trajectories (>90°or <-90°, fewer than 1% of bouts across all ages) were excluded from analysis. The displacement across each pair of frames at speeds above 5 mm·sec^{-1} were summed to find net bout displacement. Attack angle was defined as the difference between trajectory and posture of a larva at the peak speed of a bout, such that a larvae pointed horizontally and moving vertically upwards had an attack angle of 90°. Posture change during a bout was defined as the difference in body orientation observed 25 and 75 msec before peak speed, when rotations correlate with changes to trajectory [29].

Instantaneous bout rate was defined as the inverse of the interval between the first frame exceeding 5 mm·sec^{-1} in each of two successive bouts captured in a single epoch. Durations of bouts were calculated by linearly interpolating times crossing 5 mm·sec^{-1} on the rising and falling phases of each bout. Inter-bout duration was computed as the difference between inverse bout rate (instantaneous bout period) and bout duration. Vertical displacement during an inter-bout was computed as the difference between the vertical position of larva centroid at the end and start of each inter-bout.

A logistic function was used to fit the sigmoidal relationship between attack angle (γ) and posture change (r), based on a simple formulation,

$$\gamma(r) = \gamma_0 + \frac{\gamma_{max}}{1 + e^{-k(r-r_0)}} \quad , \tag{1}$$

in which γ_0 gives the lowest (most negative) attack angle (on average, in deg), ($\gamma_{max} + \gamma_0$) gives the largest positive attack angle (on average, in deg), and k is the steepness parameter (in deg^{-1}). From the derivative of equation (1), sigmoid maximal slope (dimensionless, found at $r = r_0$) is given by $k\gamma_{max}$ / 4. Because empirical data at all ages rose from the lower asymptote at similar values of posture change, sigmoid center position (r_0) was itself defined from a parameter for rise position (r_{rise}, posture change at which the sigmoid rises to 1/8 of its upper asymptote):

$$r_0 = \frac{kr_{rise} + log(\frac{-\gamma_0 - 7\gamma_{max}}{\gamma_0 + \gamma_{max}})}{k} \quad . \tag{2}$$

Parameter fits and confidence intervals were estimated in Matlab using a nonlinear regression-based solver (Levenberg-Marquardt) to minimize the sum of squared error between empirical and estimated attack angles given empirical posture changes. Initial parameter values were k=1 deg^{-1}, γ_0=-0.2°, γ_{max}=20°, and r_{rise}=-1°. Data were pooled across all bouts in a given group (age or utricle phenotype). To fit data from individual clutches, pools of available swim bouts were increased by including data from 48 hours of swimming, rather than 24 hours. Given that γ_0, γ_{max}, and r_{rise} exhibited no consistent or significant trend with age (Supplemental Table 1), values were fixed at means across all ages (-2.97 °, 17.02 °, and -1.11°, respectively) and sigmoid steepness was evaluated. One-parameter sigmoids fit empirical data well across development relative to four-parameter sigmoids (Supplemental Table 1).

In contrast, a one-parameter sigmoid poorly fit empirical data for *otog-/-* larvae (R^2=-0.17), which had uncorrelated attack angles and posture changes. Freeing the r_{rise} parameter gave a sigmoid with a steepness of approximately 0 that fit slightly better than mean attack angle (R^2=0.005), so fin biases for *otog-/-* and control larvae were calculated from maximal slopes of two-parameter sigmoids.

From sigmoid fits, empirical fin bias ($\hat{\alpha}$) was computed as an index of maximal sigmoid slope (slope/(1+slope)). Fin bias therefore reflected the ratio of attack angle to posture change

in a given climb. For sigmoids with positive steepness (k),

$$\hat{\alpha} = \frac{k \cdot 4.25°}{1 + k \cdot 4.25°} \quad . \tag{3}$$

In the generative swimming model (described below), commands to the fins (to generate attack angle) and body (to produce a posture change) were both calculated using the fin bias parameter ($0 \leq \alpha \leq 1$), such that attack angle and posture change had a maximal ratio of $\alpha/(1-\alpha)$. In this way, fin bias reflects the ratio of attack angle and posture change for both empirical and simulated swimming.

A single sigmoid (eq. 1) poorly fit empirical data for larvae with cerebellar lesions (R^2=0.100) but not controls (0.175). While the single sigmoid accurately fit data with positive posture changes and identified significant differences in steepness across conditions, it failed to capture the tendency in lesioned animals to pair positive attack angles with negative posture changes. Instead, these data were fit with the sum of two sigmoids, one reflected about the vertical axis:

$$\gamma_p(r) = \gamma(r) + \frac{\chi\gamma_{max}}{1 + e^{k(r+r_0)}} \quad . \tag{4}$$

The relative amplitudes of the two sigmoids were scaled by parameter χ, and the nose-up sigmoid amplitude was defined as 17.02° as for the one-parameter sigmoid. This four parameter function was fit from initial values of χ=0.5, k=1 deg^{-1}, γ_0=-5°, and r_{rise}=0°. For control larvae, the χ parameter did not significantly differ from zero (0.13±0.36), yielding a negligible contribution from the reflected sigmoid (see Results). Compared to the one-sigmoid function, the two-sigmoid function had minor effects on the goodness-of-fit and solutions for control data (R^2=0.178; k = 0.36 vs. 0.40). In contrast, for lesion data the two-sigmoid function improved goodness-of-fit (R^2=0.137), yielded a value for χ that significantly differed from zero (0.63±0.25), and drastically increased sigmoid steepness (k = 0.59 vs. 1.53 deg^{-1}).

Swimming simulation

We made a generative swimming model in Matlab to estimate how fin bias impacts balance and effort while climbing. Simulated larvae moved in two dimensions (horizontal, x, and vertical, z) by making series of swim bouts ($b = 1, ..., n$) of variable trajectory (t) and fixed displacement (1.27 mm, the mean empirical displacement across all ages). Larvae swam from an origin at (0,0) such that the position after bout b was determined by the trajectory of all preceding bouts. For the horizontal dimension, in mm:

$$x(b) = 1.27 \sum_{i=1}^{b} \cos(t(i)) \quad . \tag{5}$$

Larvae swam until traversing ≥99% of both the horizontal and vertical distances from the origin to a target, located at distance d and angle ϕ from the origin, or ($d \cdot \cos(\phi)$, $d \cdot \sin(\phi)$).

Larvae could control t during each bout through body rotation ($r(b)$) and by creating an attack angle with the pectoral fins ($\gamma(b)$). Body rotations allowed larvae to control their posture, which defined the direction of thrust. Larvae began swimming at horizontal posture (0°), meaning Θ during bout b was given by the sum of rotations during that and all preceding bouts:

$$\Theta(b) = \sum_{i=1}^{b} r(i) \quad . \tag{6}$$

For each bout, trajectory was defined as the sum of posture (Θ(b)), attack angle (γ), and a noise term (ε, defined below):

$$t(b) = \Theta(b) + \gamma(b) + \varepsilon \quad . \tag{7}$$

To steer, larvae could directly vary γ with the fins or influence Θ by rotating their bodies.

Movement noise (ε) was introduced to model motor errors and convective water currents that push larvae while they swim. Assuming finless larvae actively produce no attack angles ($\gamma = 0$; Figures 1B,1C), their empirical attack angles reflect external forces ($\varepsilon = t - \Theta$). Therefore, simulated ε for each bout was randomly drawn from a Gaussian distribution with a mean of 0 and standard deviation measured from empirical attack angles of finless larvae at 3 wpf (11.36°).

To make concerted posture changes and attack angles that steered towards a target, both r and γ were derived from a variable steering command ($c(b)$, in degrees) that provided feedback about the direction of the target. This command was defined before each bout and gave the direction of the target before the bout in egocentric terms (relative to the posture, $\Theta(b-1)$, and position of the larva ($x(b-1), z(b-1)$)). For a larva oriented towards the target, $c = 0$ such that no steering occurred. For the first bout, angle c equaled ϕ, and thereafter (for $b > 1$)

$$c(b) = tan^{-1}\left(\frac{d \cdot sin(\phi) - z(b-1)}{d \cdot cos(\phi) - x(b-1)}\right) - \Theta(b-1) \quad . \tag{8}$$

Rather than swim upside-down, model larvae were assumed to make yaw-axis turns (side-to-side) to keep the target horizontally forwards; if a larva swam past the target, its horizontal position was simply reflected about the horizontal position of the target, such that ($d \cdot cos(\phi) - x$) was always greater than 0.

Commands for attack angle (γ') and body rotation (r') were computed as complementary fractions that summed to the common steering command, c. The relative magnitude of γ' and r' was dictated by fin bias, α (defined from [0,1]), according to

$$\gamma'(b) = \alpha \cdot c(b) \tag{9}$$

and

$$r'(b) = (1-\alpha) \cdot c(b) \quad . \tag{10}$$

When $\alpha = 1$ larvae steered solely by generating attack angles with the fins, and when $\alpha = 0$ steered solely with posture changes. When α adopted intermediate values, the ratio of fin commands to body rotation commands was therefore $\alpha/(1-\alpha)$.

To transform commands (γ' and r') into kinematic variables (γ and r), we modeled physical limitations as a ceiling and floor imposed with logistic functions. These physical transfer functions for the fins and body had maximal slopes of 1 and were constrained to the origin, faithfully transforming commands over a certain range but reaching asymptotes at positive and negative extremes (Figure 5A). The fin transfer function had asymptotes defined by empirical best-fit sigmoids to attack angle vs. posture change, averaged across ages (Supplemental Table 1). The lower asymptote equaled γ_0 (-2.94°) and the upper asymptote equaled $\gamma_{max} + \gamma_0$ (14.04°). Given that the fin transfer function was also constrained to have maximal slope of 1 and pass through the origin, attack angle for a given bout was computed from the fin command according to

$$\gamma(\gamma'(b)) = -2.94° + \frac{16.98°}{1 + e^{-k(\gamma'(b)-6.64°)}} \quad , \qquad (11)$$

where $k = 0.24$ deg^{-1}. The body rotation transfer function was also constrained to have maximal slope of 1, pass through the origin, and have a range defined by the middle 99.9% of empirical body rotations (from -16.98° to 13.15°). Body rotation for a given bout was computed from the rotation command according to

$$r(r'(b)) = -9.40° + \frac{17.58°}{1 + e^{-k(r'(b)+1.92°)}} \quad , \qquad (12)$$

where $k = 0.13$ deg^{-1}.

To assess correlations of $\gamma(b)$ and $r(b)$ at age-, phenotype-, and clutch-specific values of $\hat{\alpha}$, we simulated 100,000 larvae at each fin bias swimming to 1 target at d=25 mm (half the length of the empirical tank). The direction of the target, ϕ, was randomly drawn from the positive lobe of a Gaussian distribution of mean 0 and standard deviation of 20.67° (that of trajectories of empirical bouts pooled across all ages). We also examined how deviation from horizontal, the mean of absolute value of simulated postures ($\Theta(b)$), as well as mean attack angle varied as a function of α, parameterized from 0 to 1 in increments of 0.01. Given that simulated larvae could deviate widely from horizontal, we computed circular mean posture in Matlab using CircStat [92]). After a simulated larva reached its target in n bouts, effort (E) was computed as the sum of squared steering commands,

$$E = \sum_{i=1}^{n} c(i)^2 \quad . \qquad (13)$$

For comparison, effort was also calculated as the sum of squared kinematic variables ($r(i)^2 + \gamma(i)^2$). Bootstrapped confidence intervals were measured by resampling mean absolute postures 1000 times with replacement.

Cost function derivation

Cost ($Q(\alpha)$) was calculated as a weighted sum of normalized deviation from horizontal ($\Theta^*(\alpha)$), Figure 6B) and normalized effort ($E(\alpha)$, Figure 6C), after both were interpolated 5-fold and smoothed with a 25 point sliding window. Deviation from horizontal was scaled by a balance weight coefficient ($0 \leq \beta \leq 1$) and effort was scaled by (1-β), such that

$$Q(\alpha) = \beta\, \Theta^*(\alpha) + (1-\beta) E(\alpha) \quad . \qquad (14)$$

Parameterizing β yielded a family of cost functions. Finding the fin bias at which cost was minimized gave the optimal fin bias, $\alpha^*(\beta)$. Confidence intervals on optimal fin bias were taken as the farthest neighboring values of β, larger and smaller, at which the bootstrapped 2.5 percentile of cost exceeded the minimal cost. Inferred balance weights ($\hat{\beta}$), those weights giving cost functions minimized by empirical fin biases ($\alpha^* = \hat{\alpha}$) empirical fin biases, were estimated by linear interpolation. Confidence estimates on $\hat{\beta}$ were similarly interpolated from 95% confidence intervals of α^* evaluated at 95% confidence intervals of $\hat{\alpha}$.

Statistics

Significance level was defined at 0.05. Pairwise t-tests were used to assess the effects of fin amputation on swim properties from sibling groups at both 1 and 3 wpf. Morphological properties were analyzed by One-way ANOVA assuming independence of all individual larvae. Two-way ANOVA with factors of age and clutch were used to assess effects on swim properties from larvae 1, 2, and 3 wpf, with significant main effects of age followed by Tukey's post-hoc tests. One exception was the coefficient of determination of trajectory and posture, which failed the assumption of homoscedasticity; effect of age was assessed with a non-parametric Kruskal-Wallis test.

A technical note on terminology

We use the term "attack angle" to describe the difference between the orientation of the body's long axis and the trajectory of swimming. As our fish swim in stagnant water, this trajectory is assumed to oppose the direction of flow. Our definition describes the orientation of an element's long axis relative to flow, consistent with the terminology in fluid dynamics. Our fish vary the direction of motion with respect to the body, and we are specifically interested in control of steering. Accordingly, we consider attack angles of the body because they are the consequence of forces orthogonal to the body long axis – by which the fish steer upwards and downwards. We refer to these upwards forces as "lift" and attribute them to pectoral fins by inference, based on loss of positive attack angles following fin amputation. However, we have no data that speak to fin

kinematics or the mechanics of force production; e.g. whether lift is generated by fin strokes or flow over fins due to body-mediated motion, or if the fins produce vertical thrust [9, 93].

Data sharing

Raw data and analysis code are available at http://www.schoppiklab.com/

Acknowledgments

Research was supported by the National Institute on Deafness and Communication Disorders under award DC012775 to DS and an Emerging Research Grant from Hearing Health Foundation to DE. The authors would like to thank Martha Bagnall for sharing the *otog-/-* line and Emre Aksay for sharing the *aldoca:GFF* line. The authors would like to thank Başak Sevinç, Katherine Harmon, Marie Greaney, Tim Gerson, and Shane Hunt for assistance with animal husbandry; Simon Sun for apparatus construction; Katherine Nagel, Kishore Kuchibhotla, Sam McKenzie, Kyla Hamling, Dena Goldblatt and members of the Schoppik and Nagel labs for helpful comments.

Author Contributions

Conceptualization, Methodology, Writing, Editing, Funding Acquisition: DE & DS, Investigation, Visualization: DE, Supervision: DS.

Author Competing Interests

The authors declare no competing interests.

References

1. S. H. Collins, P. G. Adamczyk, and A. D. Kuo, "Dynamic arm swinging in human walking," *Proceedings of the Royal Society B: Biological Sciences*, vol. 276, pp. 3679–3688, oct 2009.
2. O. Sporns and G. M. Edelman, "Solving Bernstein's problem: A proposal for the development of coordinated movement by selection," *Child Development*, vol. 64, no. 4, p. 960, 1993.
3. E. Thelen, "Motor development: A new synthesis.," *American Psychologist*, vol. 50, no. 2, pp. 79–95, 1995.
4. K. E. Adolph, B. I. Bertenthal, S. M. Boker, E. C. Goldfield, and E. J. Gibson, "Learning in the development of infant locomotion," *Monographs of the Society for Research in Child Development*, vol. 62, no. 3, pp. 1–162, 1997.
5. M. H. Dickinson, "How animals move: An integrative view," *Science*, vol. 288, no. 5463, pp. 100–106, 2000.
6. E. Thelen, B. D. Ulrich, and P. H. Wolff, "Hidden skills: A dynamic systems analysis of treadmill stepping during the first year," *Monographs of the Society for Research in Child Development*, vol. 56, no. 1, pp. 1–103, 1991.
7. E. von Holst, "On the nature of order in the central nervous system," in *The Behavioral Physiology of Animals and Man*, ch. 1, pp. 3–32, London: Butler and Tanner Ltd, 1973. tr. by R. Martin.
8. M. Sfakiotakis, D. Lane, and J. Davies, "Review of fish swimming modes for aquatic locomotion," *IEEE Journal of Oceanic Engineering*, vol. 24, no. 2, pp. 237–252, 1999.
9. Y. G. Aleyev, *Nekton*. Dr. W. Junk, 1977.
10. P. W. Webb, "Control of posture, depth, and swimming trajectories of fishes," *Integrative and Comparative Biology*, vol. 42, no. 1, pp. 94–101, 2002.
11. C. Wilga and G. Lauder, "Function of the heterocercal tail in sharks: quantitative wake dynamics during steady horizontal swimming and vertical maneuvering," *Journal of Experimental Biology*, vol. 205, no. 16, pp. 2365–2374, 2002.
12. M. M. Munk, "The aerodynamic forces on airship hulls," *National Advisory Committee on Aeronautics (NACA)*, vol. 184, 1924.
13. J. J. Magnuson, "Hydrostatic equilibrium of euthynnus affinis, a pelagic teleost without a gas bladder," *Copeia*, vol. 1970, no. 1, pp. 56–85, 1970.
14. F. Ullén, T. G. Deliagina, G. N. Orlovsky, and S. Grillner, "Spatial orientation in the lamprey. i. control of pitch and roll," *Journal of Experimental Biology*, vol. 198, no. 3, pp. 665–673, 1995.
15. M. W. Bagnall and D. L. McLean, "Modular organization of axial microcircuits in zebrafish," *Science*, vol. 343, no. 6167, pp. 197–200, 2014.
16. D. E. Ehrlich and D. Schoppik, "Control of movement initiation underlies the development of balance," *Current Biology*, vol. 27, no. 3, pp. 334–344, 2017.
17. M. H. Green, R. K. Ho, and M. E. Hale, "Movement and function of the pectoral fins of the larval zebrafish (danio rerio) during slow swimming," *Journal of Experimental Biology*, vol. 214, no. 18, pp. 3111–3123, 2011.
18. M. E. Hale, "Developmental change in the function of movement systems: Transition of the pectoral fins between respiratory and locomotor roles in zebrafish," *Integrative and Comparative Biology*, vol. 54, no. 2, pp. 238–249, 2014.
19. D. M. Parichy, M. R. Elizondo, M. G. Mills, T. N. Gordon, and R. E. Engeszer, "Normal table of postembryonic zebrafish development: Staging by externally visible anatomy of the living fish," *Developmental Dynamics*, vol. 238, no. 12, pp. 2975–3015, 2009.
20. J. C. Marques, S. Lackner, R. Félix, and M. B. Orger, "Structure of the zebrafish locomotor repertoire revealed with unsupervised behavioral clustering," *Current Biology*, vol. 28, no. 2, pp. 181–195.e5, 2018.
21. R. Roberts, J. Elsner, and M. W. Bagnall, "Delayed otolith development does not impair vestibular circuit formation in zebrafish," *Journal of the Association for Research in Otolaryngology*, vol. 18, pp. 415–425, mar 2017.
22. E. Todorov and M. I. Jordan, "Optimal feedback control as a theory of motor coordination," *Nature Neuroscience*, vol. 5, no. 11, pp. 1226–1235, 2002.
23. I. O'Sullivan, E. Burdet, and J. Diedrichsen, "Dissociating variability and effort as determinants of coordination," *PLoS Computational Biology*, vol. 5, no. 4, p. e1000345, 2009.
24. D. H. Thorsen, J. J. Cassidy, and M. E. Hale, "Swimming of larval zebrafish: fin-axis coordination and implications for function and neural control," *Journal of Experimental Biology*, vol. 207, no. 24, pp. 4175–4183, 2004.
25. M. H. Green and M. E. Hale, "Activity of pectoral fin motoneurons during two swimming gaits in the larval zebrafish (danio rerio) and localization of upstream circuit elements," *Journal of Neurophysiology*, vol. 108, no. 12, pp. 3393–3402, 2012.

26. W. J. Stewart and M. J. McHenry, "Sensing the strike of a predator fish depends on the specific gravity of a prey fish," *Journal of Experimental Biology*, vol. 213, no. 22, pp. 3769–3777, 2010.
27. M. W. Bagnall and D. Schoppik, "Development of vestibular behaviors in zebrafish," *Current Opinion in Neurobiology*, vol. 53, pp. 83–89, 2018.
28. E. G. Drucker, "Wake dynamics and locomotor function in fishes: Interpreting evolutionary patterns in pectoral fin design," *Integrative and Comparative Biology*, vol. 42, no. 5, pp. 997–1008, 2002.
29. D. E. Ehrlich and D. Schoppik, "A novel mechanism for volitional locomotion in larval zebrafish," *bioRxiv*, 2017.
30. W. Braemer and H. Braemer, "Orientation of fish to gravity," *Limnology and Oceanography*, vol. 3, no. 4, pp. 362–372, 1958.
31. W. Mo, F. Chen, A. Nechiporuk, and T. Nicolson, "Quantification of vestibular-induced eye movements in zebrafish larvae," *BMC Neuroscience*, vol. 11, no. 1, p. 110, 2010.
32. M. Cohen-Salmon, A. El-Amaroui, M. Leibovici, and C. Petit, "Otogelin: A glycoprotein specific to the acellular membranes of the innerfitear," *Proceedings of the National Academy of Sciences*, vol. 94, no. 26, pp. 14450–14455, 1997.
33. G. A. Stooke-Vaughan, N. D. Obholzer, S. Baxendale, S. G. Megason, and T. T. Whitfield, "Otolith tethering in the zebrafish otic vesicle requires otogelin and -tectorin," *Development*, vol. 142, no. 6, pp. 1137–1145, 2015.
34. W. T. Thach, H. Goodkin, and J. Keating, "The cerebellum and the adaptive coordination of movement," *Annual review of neuroscience*, vol. 15, no. 1, pp. 403–442, 1992.
35. S. d. Lac, J. L. Raymond, T. J. Sejnowski, and S. G. Lisberger, "Learning and memory in the vestibulo-ocular reflex," *Annual review of neuroscience*, vol. 18, no. 1, pp. 409–441, 1995.
36. J. Altman and S. A. Bayer, *Development of the cerebellar system: in relation to its evolution, structure, and functions*. CRC, 1997.
37. M. Hashimoto and M. Hibi, "Development and evolution of cerebellar neural circuits," *Development, Growth & Differentiation*, vol. 54, pp. 373–389, apr 2012.
38. F. D. Bene, C. Wyart, E. Robles, A. Tran, L. Looger, E. K. Scott, E. Y. Isacoff, and H. Baier, "Filtering of visual information in the tectum by an identified neural circuit," *Science*, vol. 330, pp. 669–673, oct 2010.
39. K. R. Hamling, Z. J. Tobias, and T. A. Weissman, "Mapping the development of cerebellar purkinje cells in zebrafish," *Developmental Neurobiology*, vol. 75, pp. 1174–1188, feb 2015.
40. M. Takeuchi, K. Matsuda, S. Yamaguchi, K. Asakawa, N. Miyasaka, P. Lal, Y. Yoshihara, A. Koga, K. Kawakami, T. Shimizu, and M. Hibi, "Establishment of gal4 transgenic zebrafish lines for analysis of development of cerebellar neural circuitry," *Developmental Biology*, vol. 397, no. 1, pp. 1–17, 2015.
41. E. Guigon, P. Baraduc, and M. Desmurget, "Computational motor control: Redundancy and invariance," *Journal of Neurophysiology*, vol. 97, pp. 331–347, jan 2007.
42. P. W. Webb, "The biology of fish swimming," *Mechanics and physiology of animal swimming*, vol. 4562, 1994.
43. J. L. van Leeuwen, C. J. Voesenek, and U. K. Müller, "How body torque and strouhal number change with swimming speed and developmental stage in larval zebrafish," *Journal of The Royal Society Interface*, vol. 12, no. 110, p. 20150479, 2015.
44. D. Thorsen and M. Hale, "Development of zebrafish (danio rerio) pectoral fin musculature," *Journal of Morphology*, vol. 266, no. 2, pp. 241–255, 2005.
45. R. W. IV, N. Neubarth, and M. E. Hale, "The function of fin rays as proprioceptive sensors in fish," *Nature Communications*, vol. 4, apr 2013.
46. B. R. Aiello, M. W. Westneat, and M. E. Hale, "Mechanosensation is evolutionarily tuned to locomotor mechanics," *Proceedings of the National Academy of Sciences*, vol. 114, pp. 4459–4464, apr 2017.
47. S. H. Collins, M. Wisse, and A. Ruina, "A three-dimensional passive-dynamic walking robot with two legs and knees," *The International Journal of Robotics Research*, vol. 20, pp. 607–615, jul 2001.
48. U. Proske and S. C. Gandevia, "The proprioceptive senses: Their roles in signaling body shape, body position and movement, and muscle force," *Physiological Reviews*, vol. 92, pp. 1651–1697, oct 2012.
49. J. C. Tuthill and R. I. Wilson, "Mechanosensation and adaptive motor control in insects," *Current Biology*, vol. 26, pp. R1022–R1038, oct 2016.
50. S. Knafo and C. Wyart, "Active mechanosensory feedback during locomotion in the zebrafish spinal cord," *Current Opinion in Neurobiology*, vol. 52, pp. 48–53, oct 2018.
51. D. Combes, D. L. Ray, F. M. Lambert, J. Simmers, and H. Straka, "An intrinsic feed-forward mechanism for vertebrate gaze stabilization," *Current Biology*, vol. 18, pp. R241–R243, mar 2008.
52. G. Orlovsky, T. Deliagina, and P. Walln, "Vestibular control of swimming in lamprey," *Experimental Brain Research*, vol. 90, sep 1992.
53. S. Timerick, D. Paul, and B. Roberts, "Dynamic characteristics of vestibular-driven compensatory fin movements of the dogfish," *Brain Research*, vol. 516, pp. 318–321, may 1990.
54. M. I. Coates, "The origin of vertebrate limbs," *Development*, vol. 1994, no. Supplement, pp. 169–180, 1994.
55. N. H. Shubin, E. B. Daeschler, and F. A. Jenkins, "The pectoral fin of tiktaalik roseae and the origin of the tetrapod limb," *Nature*, vol. 440, pp. 764–771, apr 2006.
56. H. Jung, M. Baek, K. P. D'Elia, C. Boisvert, P. D. Currie, B.-H. Tay, B. Venkatesh, S. M. Brown, A. Heguy, D. Schoppik, and J. S. Dasen, "The ancient origins of neural substrates for land walking," *Cell*, vol. 172, pp. 667–682.e15, feb 2018.
57. A. Flock, "Structure of the macula utriculi with special reference to directional interplay of sensory responses as revealed by morphological polarization," *The Journal of Cell Biology*, vol. 22, no. 2, pp. 413–431, 1964.
58. X. j. Yu, J. D. Dickman, and D. E. Angelaki, "Detection thresholds of macaque otolith afferents," *Journal of Neuroscience*, vol. 32, no. 24, pp. 8306–8316, 2012.
59. D. Schoppik, I. H. Bianco, D. A. Prober, A. D. Douglass, D. N. Robson, J. M. Li, J. S. Greenwood, E. Soucy, F. Engert, and A. F. Schier, "Gaze-stabilizing central vestibular neurons project asymmetrically to extraocular motoneuron pools," *The Journal of Neuroscience*, vol. 37, pp. 11353–11365, sep 2017.
60. I. H. Bianco, L.-H. Ma, D. Schoppik, D. N. Robson, M. B. Orger, J. C. Beck, J. M. Li, A. F. Schier, F. Engert, and R. Baker, "The tangential nucleus controls a gravito-inertial vestibulo-ocular reflex," *Current Biology*, vol. 22, no. 14, pp. 1285–1295, 2012.

61. K. E. Severi, R. Portugues, J. C. Marques, D. M. O'Malley, M. B. Orger, and F. Engert, "Neural control and modulation of swimming speed in the larval zebrafish," *Neuron*, vol. 83, pp. 692–707, aug 2014.
62. T. R. Thiele, J. C. Donovan, and H. Baier, "Descending control of swim posture by a midbrain nucleus in zebrafish," *Neuron*, vol. 83, pp. 679–691, aug 2014.
63. W.-C. Wang and D. L. McLean, "Selective responses to tonic descending commands by temporal summation in a spinal motor pool," *Neuron*, vol. 83, pp. 708–721, aug 2014.
64. L.-H. Ma, E. Gilland, A. H. Bass, and R. Baker, "Ancestry of motor innervation to pectoral fin and forelimb," *Nature Communications*, vol. 1, pp. 1–8, jul 2010.
65. H. Suwa, E. Gilland, and R. Baker, "Otolith ocular reflex function of the tangential nucleus in teleost fish," *Annals of the New York Academy of Sciences*, vol. 871, no. 1, pp. 1–14, 1999.
66. J. Laurens, S. Liu, X.-J. Yu, R. Chan, D. Dickman, G. C. DeAngelis, and D. E. Angelaki, "Transformation of spatiotemporal dynamics in the macaque vestibular system from otolith afferents to cortex," *eLife*, vol. 6, 2017.
67. S. M. Morton and A. J. Bastian, "Cerebellar control of balance and locomotion," *The Neuroscientist*, vol. 10, pp. 247–259, jun 2004.
68. W. Thach, "A role for the cerebellum in learning movement coordination," *Neurobiology of Learning and Memory*, vol. 70, pp. 177–188, jul 1998.
69. A. J. Bastian, "Learning to predict the future: the cerebellum adapts feedforward movement control," *Current Opinion in Neurobiology*, vol. 16, pp. 645–649, dec 2006.
70. M. Manto, J. M. Bower, A. B. Conforto, J. M. Delgado-García, S. N. F. da Guarda, M. Gerwig, C. Habas, N. Hagura, R. B. Ivry, P. Marin, M. Molinari, E. Naito, D. A. Nowak, N. O. B. Taib, D. Pelisson, C. D. Tesche, C. Tilikete, and D. Timmann, "Consensus paper: Roles of the cerebellum in motor control—the diversity of ideas on cerebellar involvement in movement," *The Cerebellum*, vol. 11, pp. 457–487, dec 2011.
71. H. Matsui, K. Namikawa, A. Babaryka, and R. W. Koster, "Functional regionalization of the teleost cerebellum analyzed in vivo," *Proceedings of the National Academy of Sciences*, vol. 111, pp. 11846–11851, jul 2014.
72. L. D. Knogler, A. M. Kist, and R. Portugues, "Motor context dominates output from purkinje cell functional regions during reflexive visuomotor behaviours," *eLife*, vol. 8, jan 2019.
73. I. A. Favre-Bulle, G. Vanwalleghem, M. A. Taylor, H. Rubinsztein-Dunlop, and E. K. Scott, "Cellular-resolution imaging of vestibular processing across the larval zebrafish brain," *Current Biology*, vol. 28, pp. 3711–3722.e3, dec 2018.
74. G. Migault, T. L. van der Plas, H. Trentesaux, T. Panier, R. Candelier, R. Proville, B. Englitz, G. Debrégeas, and V. Bormuth, "Whole-brain calcium imaging during physiological vestibular stimulation in larval zebrafish," *Current Biology*, vol. 28, pp. 3723–3735.e6, dec 2018.
75. D. H. Paul and B. L. Roberts, "The significance of cerebellar function for a reflex movement of the dogfish," *Journal of Comparative Physiology ? A*, vol. 134, no. 1, pp. 69–74, 1979.
76. A. S. Machado, D. M. Darmohray, J. Fayad, H. G. Marques, and M. R. Carey, "A quantitative framework for whole-body coordination reveals specific deficits in freely walking ataxic mice," *eLife*, vol. 4, oct 2015.
77. S. Grillner and P. Wallén, "Innate versus learned movements—a false dichotomy?," in *Progress in Brain Research*, pp. 1–12, Elsevier, 2004.
78. M. Beraneck, F. M. Lambert, and S. G. Sadeghi, "Functional development of the vestibular system," in *Development of Auditory and Vestibular Systems*, pp. 449–487, Elsevier, 2014.
79. D. E. Angelaki, E. M. Klier, and L. H. Snyder, "A vestibular sensation: Probabilistic approaches to spatial perception," *Neuron*, vol. 64, no. 4, pp. 448–461, 2009.
80. K. P. Körding and D. M. Wolpert, "Bayesian integration in sensorimotor learning," *Nature*, vol. 427, no. 6971, pp. 244–247, 2004.
81. J. Izawa, T. Rane, O. Donchin, and R. Shadmehr, "Motor adaptation as a process of reoptimization," *Journal of Neuroscience*, vol. 28, no. 11, pp. 2883–2891, 2008.
82. L. Rigoux and E. Guigon, "A model of reward- and effort-based optimal decision making and motor control," *PLoS Computational Biology*, vol. 8, no. 10, p. e1002716, 2012.
83. P. N. Kugler, J. S. Kelso, and M. Turvey, "1 on the concept of coordinative structures as dissipative structures: I. theoretical lines of convergence," in *Advances in Psychology*, pp. 3–47, Elsevier, 1980.
84. N. A. Bernstein, *The co-ordination and regulation of movements*. Pergamon Press Ltd., 1967.
85. K. M. Newell and P. V. McDonald, "Learning to coordinate redundant biomechanical degrees of freedom," in *Interlimb Coordination*, pp. 515–536, Elsevier, 1994.
86. E. Thelen, "Learning to walk: Ecological demands and phylogenetic constraints.," *Advances in infancy research*, 1984.
87. M. H. Woollacott, A. Shumway-Cook, and H. G. Williams, "The development of posture and balance control in children," *Development of posture and gait across the life span*, pp. 77–96, 1989.
88. G. Yogev-Seligmann, J. M. Hausdorff, and N. Giladi, "Do we always prioritize balance when walking? towards an integrated model of task prioritization," *Movement Disorders*, vol. 27, no. 6, pp. 765–770, 2012.
89. K. E. Adolph, "Learning to learn in the development of action," in *Action as an organizer of perception and cognition during learning and development: Minnesota Symposium on Child Development*, vol. 33, pp. 91–122, 2016.
90. T. Whitfield, M. Granato, F. van Eeden, U. Schach, M. Brand, M. Furutani-Seiki, P. Haffter, M. Hammerschmidt, C. Heisenberg, Y. Jiang, D. Kane, R. Kelsh, M. Mullins, J. Odenthal, and C. Nusslein-Volhard, "Mutations affecting development of the zebrafish inner ear and lateral line," *Development*, vol. 123, pp. 241–254, 1996.
91. J. Schindelin, I. Arganda-Carreras, E. Frise, V. Kaynig, M. Longair, T. Pietzsch, S. Preibisch, C. Rueden, S. Saalfeld, B. Schmid, J.-Y. Tinevez, D. J. White, V. Hartenstein, K. Eliceiri, P. Tomancak, and A. Cardona, "Fiji: an open-source platform for biological-image analysis," *Nature Methods*, vol. 9, pp. 676–682, jun 2012.
92. P. Berens, "CircStat: A MATLAB toolbox for circular statistics," *Journal of Statistical Software*, vol. 31, no. 10, 2009.
93. M. Westneat, D. Thorsen, J. Walker, and M. Hale, "Structure, function, and neural control of pectoral fins in fishes," *IEEE Journal of Oceanic Engineering*, vol. 29, no. 3, pp. 674–683, 2004.

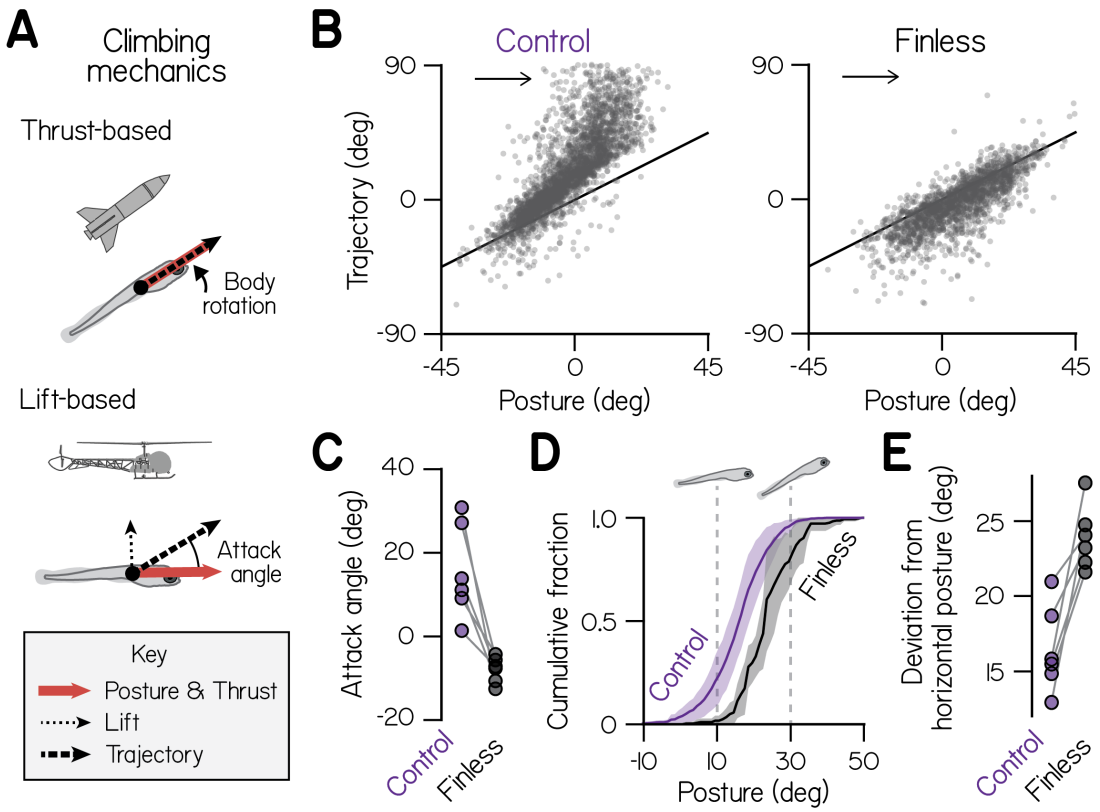

Figure 1: Larvae climb using bodies and pectoral fins. (A) Schematic of hydrostatic climbing mechanics. Like a rocket, a larva generates thrust in the direction it points (*top*), enabling it to generate upwards trajectories by rotating upwards to adopt nose-up postures. Complementarily, it may generate lift like a helicopter (*bottom*), creating an attack angle between trajectory and posture. (B) Trajectory of individual swim bouts as a function of posture, for control (2912 bouts) and finless larvae (1890 bouts). The unity line corresponds to 0 attack angle. Arrows indicate the location of bouts with large positive attack angles. (C) Mean attack angles for control and finless siblings from 6 clutches (pairwise t-test, $t_5 = 4.55$, $p = 0.0061$). (D) Cumulative fractions of postures during climbs with trajectories greater than 20°, for control and finless siblings, plotted as mean±S.D. across clutches. (E) Absolute deviation of posture from horizontal during climbs in (D) for control and finless siblings ($t_5 = 5.02$, $p = 0.0040$).

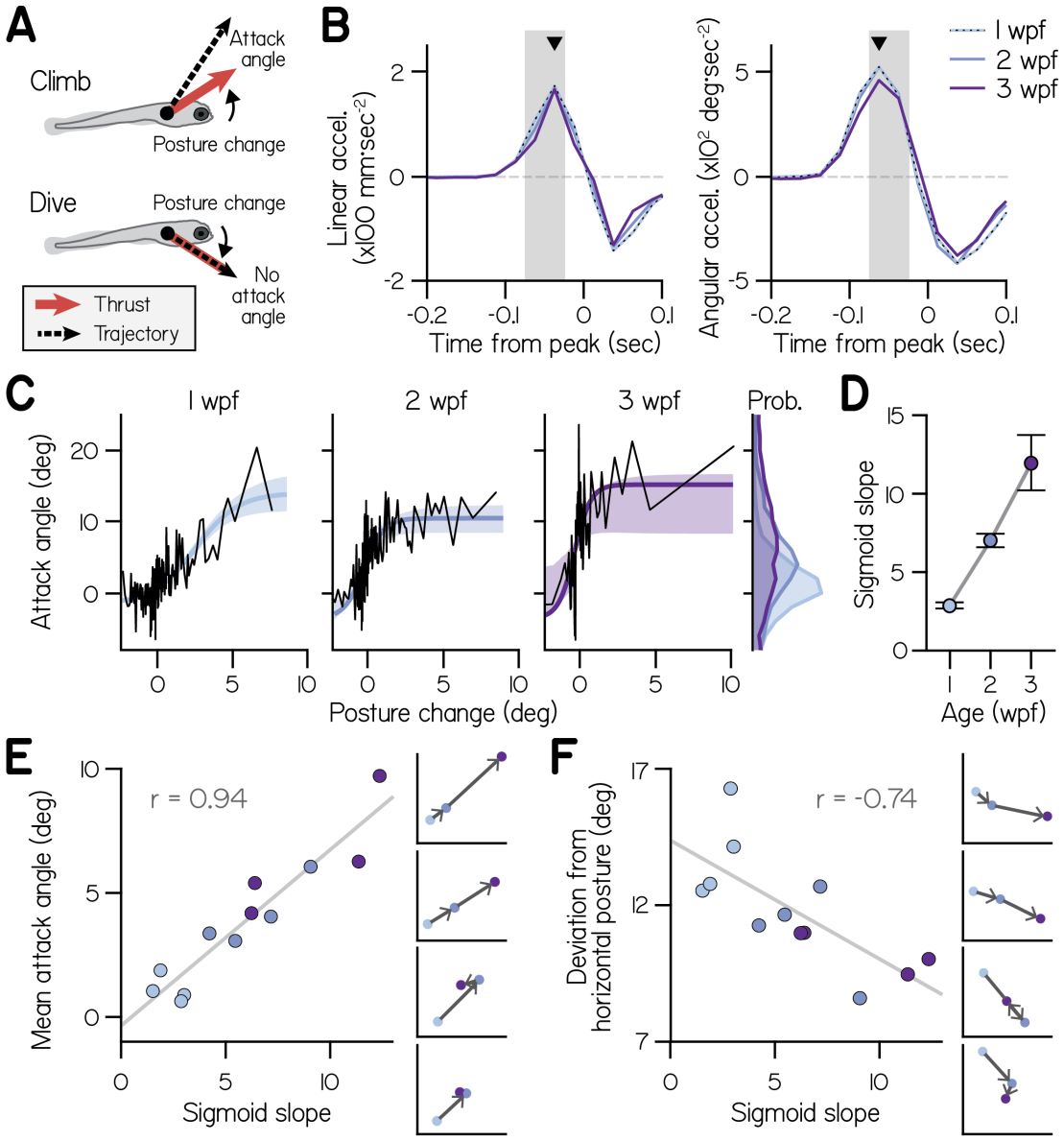

Figure 2: Development of fin-body coordination. (A) Schematic of fin-body coordination for climbing. Positive posture changes are paired with positive attack angles and negative body rotations with no attack angle, reflecting exclusion of the fins. (B) Mean linear and angular acceleration during swim bouts at 1, 2, and 3 weeks post-fertilization (wpf), temporally aligned to peak linear speed (time 0). The window used to compute posture change is highlighted in gray. (C) Attack angle as a function of posture change for bouts at 1, 2, and 3 wpf, with cropped attack angle probability distributions (*right*). Data plotted as means of equally-sized bins (black lines) and superimposed with best-fit sigmoids and their bootstrapped S.D. (D) Maximal slopes of best-fit sigmoids plotted with 95% confidence intervals as a function of age. (E,F) Mean attack angle (E) and absolute deviation from horizontal (F) for each clutch and age, evaluated over 48 hours, are plotted as functions of maximal sigmoid slope with Pearson's correlation coefficients (r; p=5.6E-6 for attack angle and p=6.3E-3 for deviation from horizontal). Developmental trajectories for four individual clutches are plotted on identical axes (*right*).

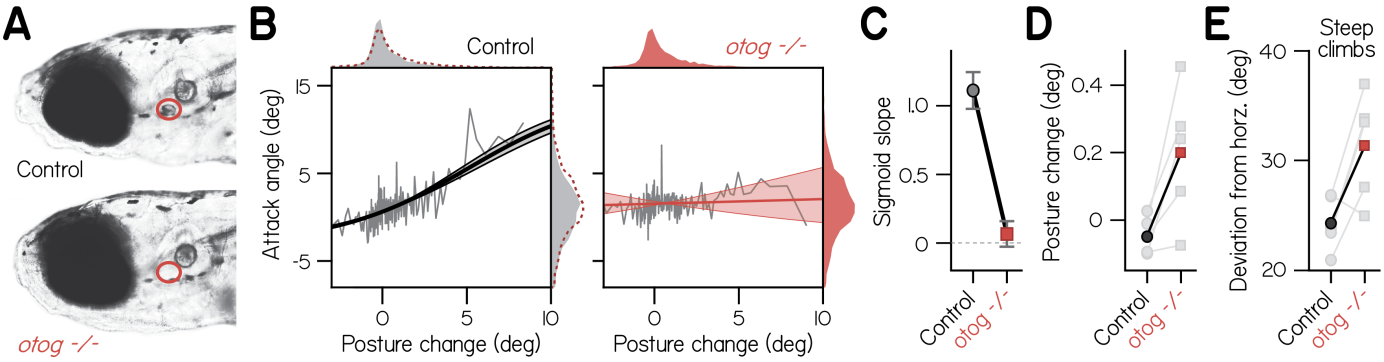

Figure 3: Fin-body coordination is abolished by peripheral vestibular lesion. (A) Representative lateral photomicrographs, one of a larva with typical development of utricular (anterior) otoliths (*top*, control: wild-type or heterozygous for *otogelin*) and another of its sibling lacking utricular otoliths (*bottom*, *otog -/-*). Utricle position is encircled in red. (B) Attack angle as a function of posture change for bouts by control larvae (4,767 bouts) and *otog-/-* siblings (3,656 bouts). Data plotted as means of equally-sized bins (gray lines) superimposed with best-fit sigmoids and their bootstrapped S.D. Marginals show cropped probability distributions, with *otog-/-* marginals superimposed on control data as dashed lines. (C) Maximal slopes of best-fit sigmoids plotted with 95% confidence intervals. (D) Median posture change during bouts by individual clutches (gray) and their means. Pairwise t-test, $t_4 = 3.13$, $p = 0.035$. (E) Mean deviation of posture from horizontal during steep climbs (> 20°). Pairwise t-test, $t_4 = 3.02$, $p = 0.039$.

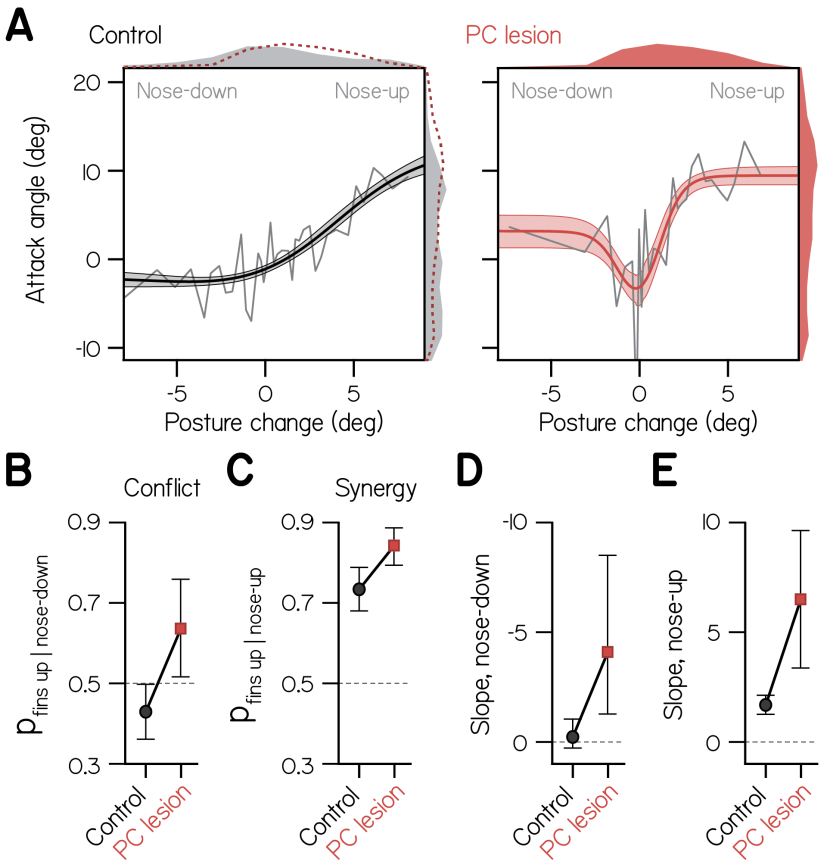

Figure 4: Cerebellar lesion impairs fin-body coordination. (A) Attack angle as a function of posture change for bouts by control larvae (602 bouts) and siblings with lesioned Purkinje cells (408 bouts). Data plotted as means of equally-sized bins (gray lines) superimposed with best-fit sum of two sigmoids and their bootstrapped S.D. Marginals show cropped probability distributions, with marginals from lesioned larvae superimposed on control data as dashed lines. (B) Proportion of bouts with attack angles more positive than 1 wpf baseline (-1.59°) given nose-down posture change (<-1°), with bootstrapped 95% CI. (C) Proportion of bouts with attack angles more positive than 1 wpf baseline (-1.59°) given nose-up posture change (>1°), with bootstrapped 95% CI. (D,E) Largest magnitude slopes of the nose-down (D) and nose-up (E) best-fit sigmoids to data in (A), with bootstrapped 95% CI.

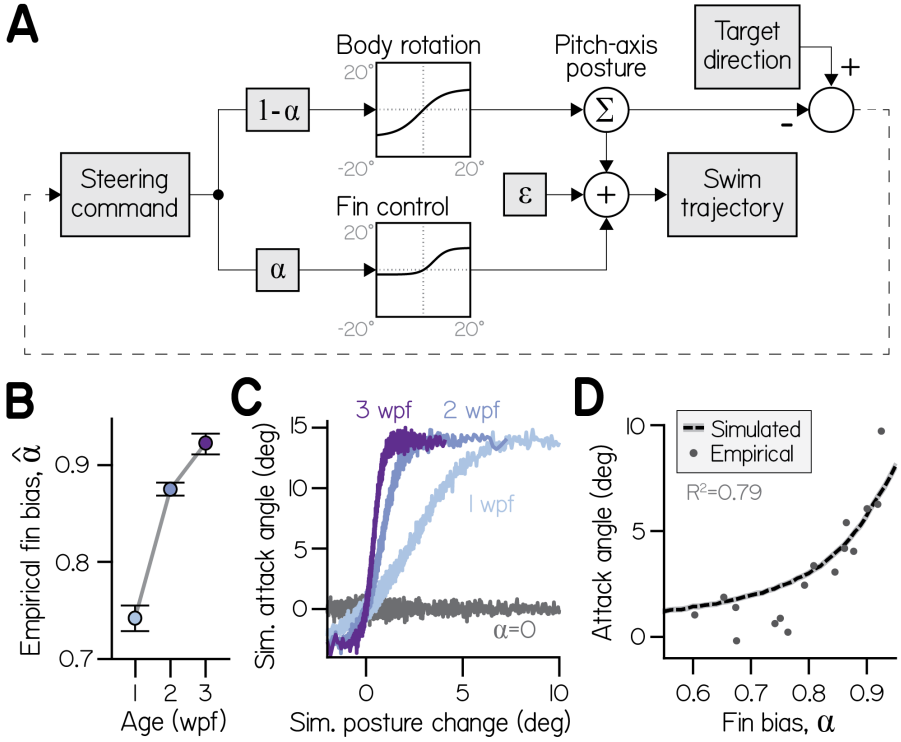

Figure 5: A one-parameter control system captures fin-body coordination *in silico*. (A) Circuit diagram to transform pitch-axis steering commands into climbing swims using the body and pectoral fins. Steering commands are defined by the direction of a target in egocentric coordinates. The relative weight of commands to rotate the body (to direct thrust) and produce an attack angle with the fins (by generating lift) is dictated by fin bias (α). To model physical transformations from commands into kinematic variables, commands to the body and fins are filtered to impose empirically-derived ceilings and floors on posture changes and attack angles (see Methods). Swim trajectory is defined by posture (fish propel where they point) but modified by attack angle and error (ε). (B) Empirical fin bias ($\hat{\alpha}$), computed from maximal sigmoid slope (slope/(1+slope)), as a function of age with 95% confidence intervals. (C) Attack angle as a function of posture change, plotted as means of equally-sized bins. Climbs to 100,000 targets were simulated using empirical fin bias ($\hat{\alpha}$) from 1, 2, and 3 wpf larvae, and at $\alpha = 0$ for comparison. (D) Mean attack angle for simulated larvae with parameterized fin bias (line), superimposed on empirical attack angles and fin biases ($\hat{\alpha}$) for each clutch at each age. Simulated attack angles at $\hat{\alpha}$ account for 79% of variation in empirically observed attack angles (R^2).

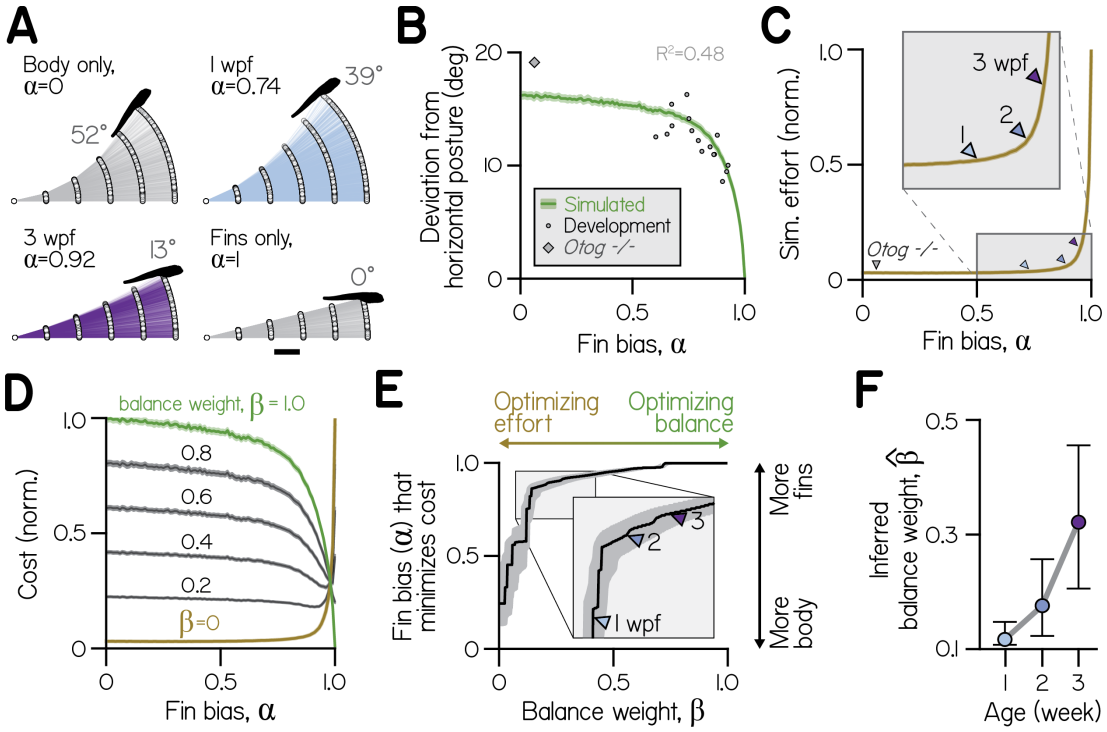

Figure 6: Effects of fin-body coordination on balance-effort trade-off. (A) Trajectories (lines) and initial positions (dots) of bouts simulated with the control system in (A) at fin biases of 0, 0.74 ($\hat{\alpha}$ at 1 wpf), 0.92 ($\hat{\alpha}$ at 3 wpf), and 1.0, for 1000 larvae swimming towards targets 25 μm away. Posture following the fifth bout of the steepest climb is superimposed. Scale bar equals 1 mm. (B) Simulated absolute deviation from horizontal posture as a function of α, plotted as mean (green line) and bootstrapped 99% confidence intervals (shaded band). Data are superimposed on empirical values for individual clutches of a given age (circles, *Development*, R^2=0.48) and *otog-/-* larvae (diamond). (C) Effort, the sum of squared motor commands to the body and fins, from simulations in (B) normalized and plotted as a function of α as mean (line) and bootstrapped 99% confidence intervals (shaded band). Empirical fin biases at 1, 2, and 3 wpf and for *otog-/-* larvae are indicated with triangles. (D) Cost as a function of fin bias, computed as sums of normalized curves in (B) and (C) weighted by β (balance weight) and $(1-\beta)$, respectively (*left*). When $\beta = 1$ (green), cost is equivalent to normalized deviation from horizontal. When $\beta = 0$ (ochre), cost is equivalent to effort. Intermediate cost functions are plotted for β increasing by 0.2, with 99% confidence interval (shaded band). (E) Fin bias at which cost was minimized is plotted at each value of balance weight, with 95% confidence intervals. (F) Inferred balance weight ($\hat{\beta}$) is plotted as a function of age, with 95% confidence intervals. This weight gives the cost function minimized by empirical fin bias at a given age (from the curve in E).

Supplemental Figures

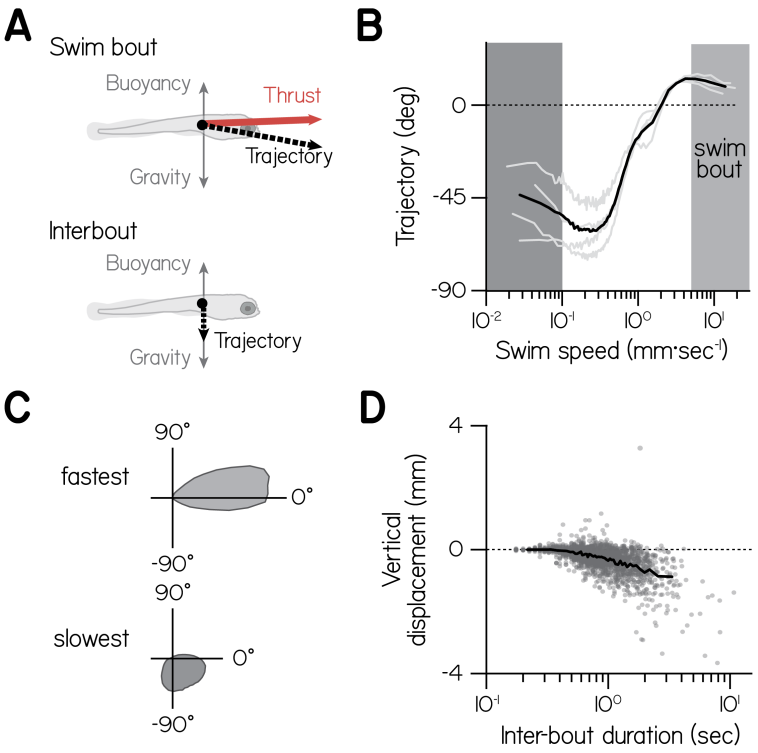

Figure S1. Larvae tend to sink between bouts. (A) Schematic of hydrostatic forces acting on larvae absent lift during bouts (*top*) and between bouts (*bottom*). (B) Trajectory as a function of swim speed, plotted as means of equally-sized bins for 4 clutches (gray lines) and their mean (black). Swim bouts (light gray band, speeds faster than 5 mm·sec^{-1}) tended slightly upwards, while larvae sank at slow speeds, particularly slower than 0.1 mm·sec^{-1} (dark gray band). (C) Polar probability distributions of trajectories during swim bouts (light gray, *top*) and at speeds slower than 0.1 mm·sec^{-1} (dark gray, *bottom*). (D) Vertical displacement during the interval between two bouts (when speed decreased below 5mm·sec^{-1}) as a function of interval duration, for individual bouts and mean of equally-sized bins.

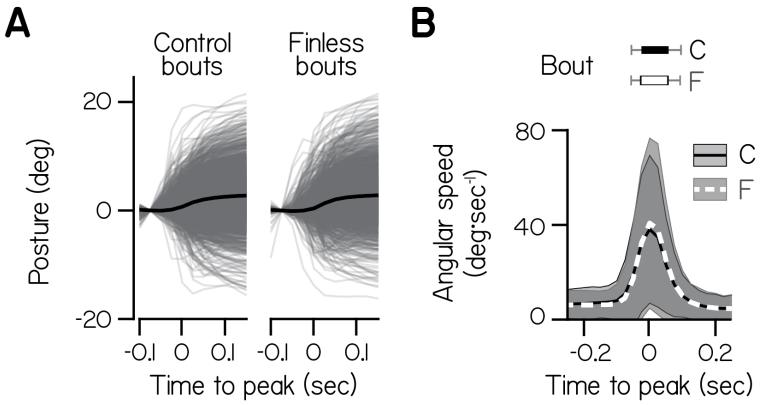

Figure S2. Posture as a function of time during individual bouts (gray lines) and their mean (black) by control and finless siblings. Data were aligned to peak speed at time 0 and baseline subtracted at -0.75 sec. (B) Angular speed as a function of time during bouts (*bottom*), plotted as mean and S.D., for control and finless siblings. Durations when speed exceeded 5 mm·sec^{-1} are plotted for control and finless larvae (top) as median and 95% confidence interval.

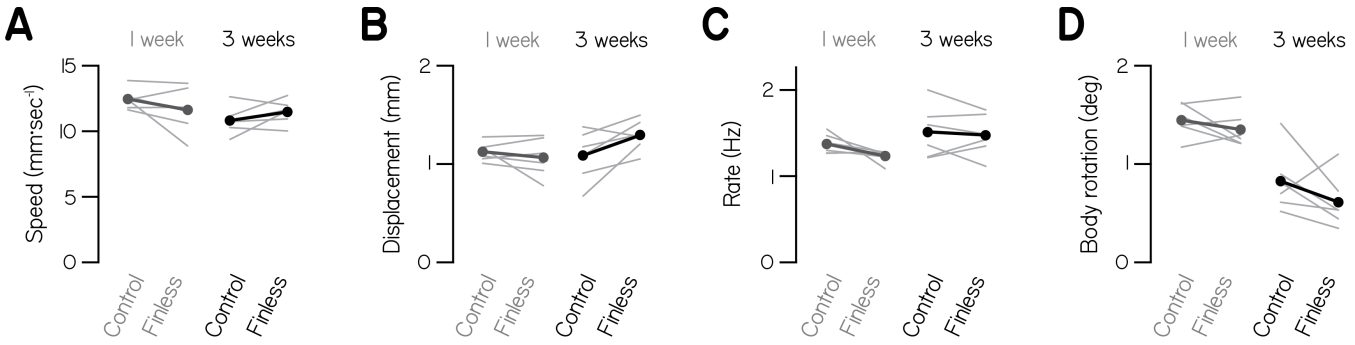

Figure S3. Basic swimming statistics are unaffected by fin amputation at 1 and 3 wpf. (A-D) Mean maximum speed across bouts (A), mean net displacement (B), mean rate (C), and mean absolute body rotation (D) of swim bouts are plotted as thin lines by clutch (n=6, 8 larvae per) for larvae with amputated fins and unaltered siblings at 1 and 3 wpf. Within group means are plotted as thick lines and points.

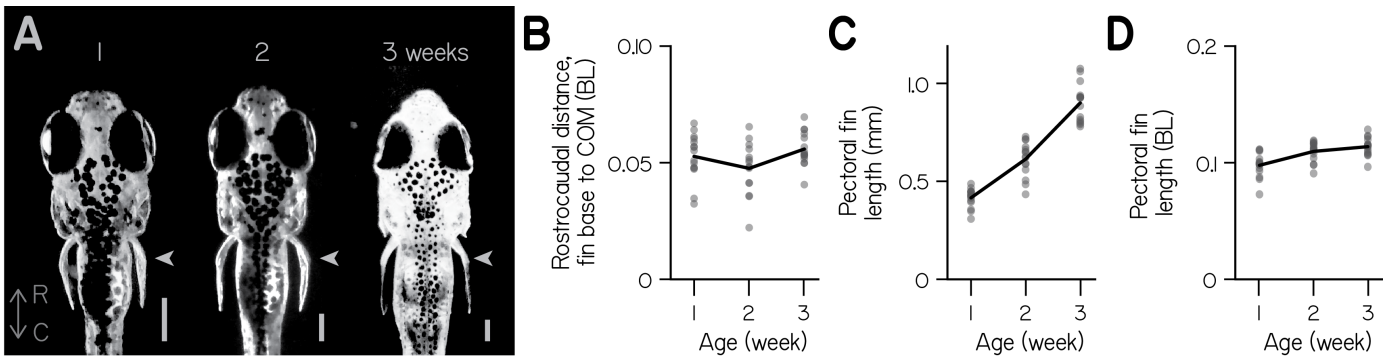

Figure S4. Pectoral fins and bodies grow proportionally. (A) Grayscale, dorsal-perspective photomicrographs of representative larvae at 1, 2, and 3 wpf, with rostrocaudal axis labeled (R-C). Pectoral fins are indicated with arrowhead. Gamma was adjusted and images scaled to comparable head length (scale bars 0.25 mm). (B) Rostrocaudal distance from base of the pectoral fins to the estimated center of mass (COM, see Methods), in body lengths (BL), as a function of age (n=15 larvae). (C) Pectoral fin length as a function of age. (D) Pectoral fin length normalized to body length as a function of age.

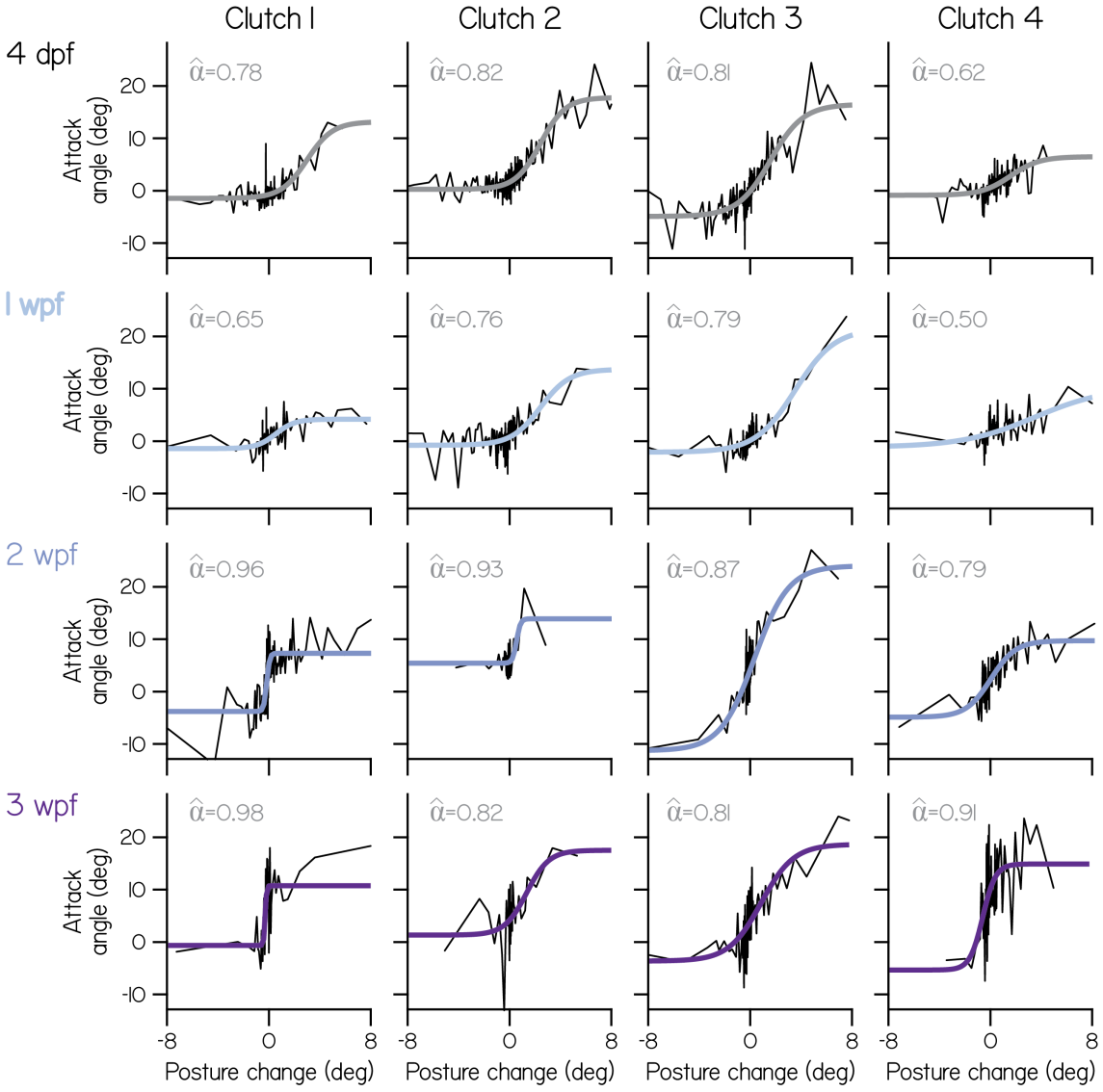

Figure S5. Clutch- and age-specific fin bias. Attack angle as a function of posture change for individual clutches (columns) at each age (rows), plotted as means of equally-sized bins, superimposed with 4 parameter sigmoid fits. Empirical fin bias ($\hat{\alpha}$), computed as an index of maximal sigmoid slope (slope/(1+slope)), is listed.

Supplemental Tables

Variable	Unit	4dpf	1wpf	2wpf	3wpf
Mean attack angle	deg	0.87	1.02	4.78	8.11
R^2 of trajectory and posture	-	0.86	0.91	0.78	0.66
Deviation from horizontal	deg	13.91	14.08	11.91	11.30
Swim bout peak speed	mm/sec	11.2	13.6	13.4	14.1
Swim bout displacement	mm	1.24	1.29	1.24	1.43
Mean bout posture change	deg	0.10	-0.23	0.24	0.21
Standard deviation of bout posture change	deg	2.21	1.84	1.84	2.10
ϱ of attack angle and body rotation	-	0.305	0.269	0.379	0.368
Proportion of climbs with trajectory >20°	-	0.26	0.30	0.34	0.43
Body length	mm	4.18	4.26	5.57	7.92
Pectoral fin length	mm	0.41	0.42	0.61	0.90
Fin distance anterior to COM	mm	0.27	0.22	0.27	0.44
Sigmoid amplitude γ_{max}	deg	19.28	15.71	14.30	18.79
Sigmoid vertical location, γ_0	deg	-3.00	-1.59	-3.72	-3.56
Sigmoid horizontal location, r_{rest}	deg	-0.77	-0.42	-1.75	-1.51
Sigmoid slope, $k \cdot \gamma_{max}/4$	-	2.76	2.89	7.03	12.01
Goodness-of-fit (R^2) for 4-parameter sigmoid ($k, \gamma_{max}, \gamma_0, r_{rest}$)	-	0.195	0.115	0.113	0.087
Goodness-of-fit (R^2) for 1-parameter sigmoid (k)	-	0.193	0.109	0.092	0.086
Empirical fin bias, $\hat{\alpha}$	-	0.73	0.74	0.88	0.92
Balance weight in cost function, β	-	0.12	0.12	0.18	0.32

Supplemental Table 1. Empirical and simulated swimming properties and morphological measurements as a function of age. Sigmoid parameters refer to the best-fit logistic function to attack angle vs. body rotation, comprising 4 degrees of freedom. ϱ: Spearman's correlation coefficient.

Variable	Unit	*otog-/-*	Control
Body length	mm	4.52±0.32	4.53±0.23
Pectoral fin length	mm	0.43±0.03	0.42±0.04
Pectoral fin length	% body length	9.6±0.6	9.3±0.8

Supplemental Table 2. Morphology of *otog-/-* larvae and control siblings (*otog*+/- and *otog*+/+ with utricles). Data listed as mean±S.D.

Variable	Unit	*otog-/-*, no utricle	utricle control	*aldoca::KR* lesioned	*aldoca::KR* control
Maximum linear speed	$mm \cdot sec^{-1}$	12.4±4.5	12.0±4.3	10.7±4.3	12.7±4.5
Duration	sec	0.084±0.034	0.079±0.033	0.109±0.070	0.120±0.051
Displacement	mm	1.23±0.61	1.13±0.54	1.25 ± 0.75	1.62±0.71
Maximal pitch-axis angular speed	$deg \cdot sec^{-1}$	98.7±73.0	90.1±69.0	84.4±54.0	100.6±61.4
Inter-bout interval	sec	1.22±1.37	1.09±1.03	2.09±2.30	2.12±2.80

Supplemental Table 3. Swim bout properties for *otog-/-* and *aldoca::KillerRed* larvae. Data listed as mean±S.D.

Supplemental Movies

Supplemental Movie 1. Lateral view of a freely-swimming, 2 wpf larva producing 4 bouts of upwards motion interleaved by periods of slow sinking.

Supplemental Movie 2. View down the long axis of a freely-swimming, 2 wpf larva producing 5 bouts of upwards motion with visible pectoral fin abduction.